BJ www.biochemj.org

BJ Structure

Biochem. J. (2009) **424**, 335–345 (Printed in Great Britain) doi:10.1042/BJ20090825

multimedia online data

A constitutively active and uninhibitable caspase-3 zymogen efficiently induces apoptosis

Jad WALTERS*, Cristina POP†, Fiona L. SCOTT†, Marcin DRAG†[1], Paul SWARTZ*, Carla MATTOS*, Guy S. SALVESEN† and A. Clay CLARK*[2]

*Department of Molecular and Structural Biochemistry, North Carolina State University, Raleigh, NC 27695, U.S.A., and †Program in Apoptosis and Cell Death, The Burnham Institute for Medical Research, 10901 N Torrey Pines Rd, La Jolla, CA 92037, U.S.A.

The caspase-3 zymogen has essentially zero activity until it is cleaved by initiator caspases during apoptosis. However, a mutation of V266E in the dimer interface activates the protease in the absence of chain cleavage. We show that low concentrations of the pseudo-activated procaspase-3 kill mammalian cells rapidly and, importantly, this protein is not cleaved nor is it inhibited efficiently by the endogenous regulator XIAP (X-linked inhibitor of apoptosis). The 1.63 Å (1 Å = 0.1 nm) structure of the variant demonstrates that the mutation is accommodated at the dimer interface to generate an enzyme with substantially the same activity and specificity as wild-type caspase-3. Structural modelling predicts that the interface mutation prevents the intersubunit linker from binding in the dimer interface, allowing the active sites to form in the procaspase in the absence of cleavage. The direct activation of procaspase-3 through a conformational switch rather than by chain cleavage may lead to novel therapeutic strategies for inducing cell death.

Key words: apoptosis, cancer therapy, conformational switch, co-operative dimer interface, procaspase activation.

INTRODUCTION

Caspase activation, more than any other event, defines a cellular response to apoptosis. Synthesized initially as zymogens (procaspases) (Figure 1A), the cytosolic pool of inactive zymogen is converted rapidly into active protease upon the induction of apoptosis. A fundamental difference exists in the caspase subfamilies regarding maturation, and this difference is a key aspect for regulating apoptosis. Initiator procaspases are stable monomers in the cell, and dimerization is facilitated following recruitment to activation platforms [1]. Importantly, once dimerized, the initiator procaspases have high enzymatic activity, and subsequent chain cleavage simply stabilizes the active site [2,3]. In contrast, the effector procaspase-3 is a stable dimer, but has very low enzymatic activity (< 0.4 % of that of the active protease) [4,5]. In this case, full activation occurs after cleavage of the IL (intersubunit linker) by initiator caspases, resulting in ordering of the active sites due to the release of two active site loops (L2 and L2′) from the IL and subsequent formation of the substrate-binding pocket (active site loop 3) (Figure 1B, and see Supplementary Movie S1 at http://www.BiochemJ.org/bj/424/0335/bj4240335add.htm). In short, the cell maintains a cytosolic pool of inactive procaspase-3 that is poised to carry out cell death.

Structural and mutational studies show that the packing of amino acid side chains in the dimer interface is intimately connected to active site formation (reviewed in [6–9]). The importance of the dimer interface was described by Wells and co-workers, who showed that allosteric inhibitors bind in the interface of the mature caspase and stabilize a form of the protein with a disorganized active site, similar to that of the procaspase [10].

In addition to small molecule binding, mutations in the allosteric site of the dimer interface were shown to affect active site formation in procaspase-3 [11]. In one case, a V266E mutation increased the activity by 60-fold, representing a pseudo-activation of the zymogen. Notably, the increase in activity did not require cleavage of the IL but rather occurred via conformational changes in the intact zymogen. This is an important consideration, because the results demonstrated that procaspase-3 can indeed gain a substantial amount of catalytic activity without cleavage of the polypeptide chain.

An understanding of procaspase dimerization and how it relates to activation will be an important step toward effective therapies for a variety of diseases that involve the dysregulation of apoptosis. Although a number of cancer treatments target proteins in the apoptotic pathways [12], most of the current therapies are upstream of caspase activation and often require combined treatments to be effective [13]. Ultimately, however, these therapies indirectly induce the activation of caspase-3. Because there is a larger pool of quiescent procaspase-3 in most cancer cells compared with normal cells [14–16], directly targeting procaspase-3 could lead to more effective therapy, since effector caspases are the terminal proteases in the cell death cascade. Overall, our results from the present study show that the dimer interface should be considered a potential target for cancer treatment, where the identification of small molecules that

Abbreviations used: Ac-DEVD-AFC, acetyl-Asp-Glu-Val-Asp-7-amino-4-trifluoromethylcoumarin; Ac-DEVD-CMK, acetyl-Asp-Glu-Val-Asp-chloromethyl ketone; bEVD-AOMK, biotinylhexanoyl-Asp-Glu-Val-acyloxymethane; D_3A, procaspase-3(D9A,D28A,D175A); D_3A,V266E, procaspase-3(D9A,D28A,D175A,V266E); HEK-293A cell, human embryonic kidney-293A cell; IL, intersubunit linker; PARP, poly(ADP-ribose) polymerase; V266E, procaspase-3(V266E); WT, wild-type procaspase-3; XIAP, X-linked inhibitor of apoptosis; Z-VAD-FMK, benzyloxycarbonyl-Val-Ala-Asp-fluoromethyl ketone.

[1]Current address: Division of Medicinal Chemistry and Microbiology, Faculty of Chemistry, Wroclaw University of Technology, Wybrzeze Wyspianskiego 27, 50-370 Wroclaw, Poland.

[2]To whom correspondence should be addressed (email clay_clark@ncsu.edu).

The atomic co-ordinates and structure factors for caspase-3(V266E) have been deposited in the PDB under accession code 3ITN.

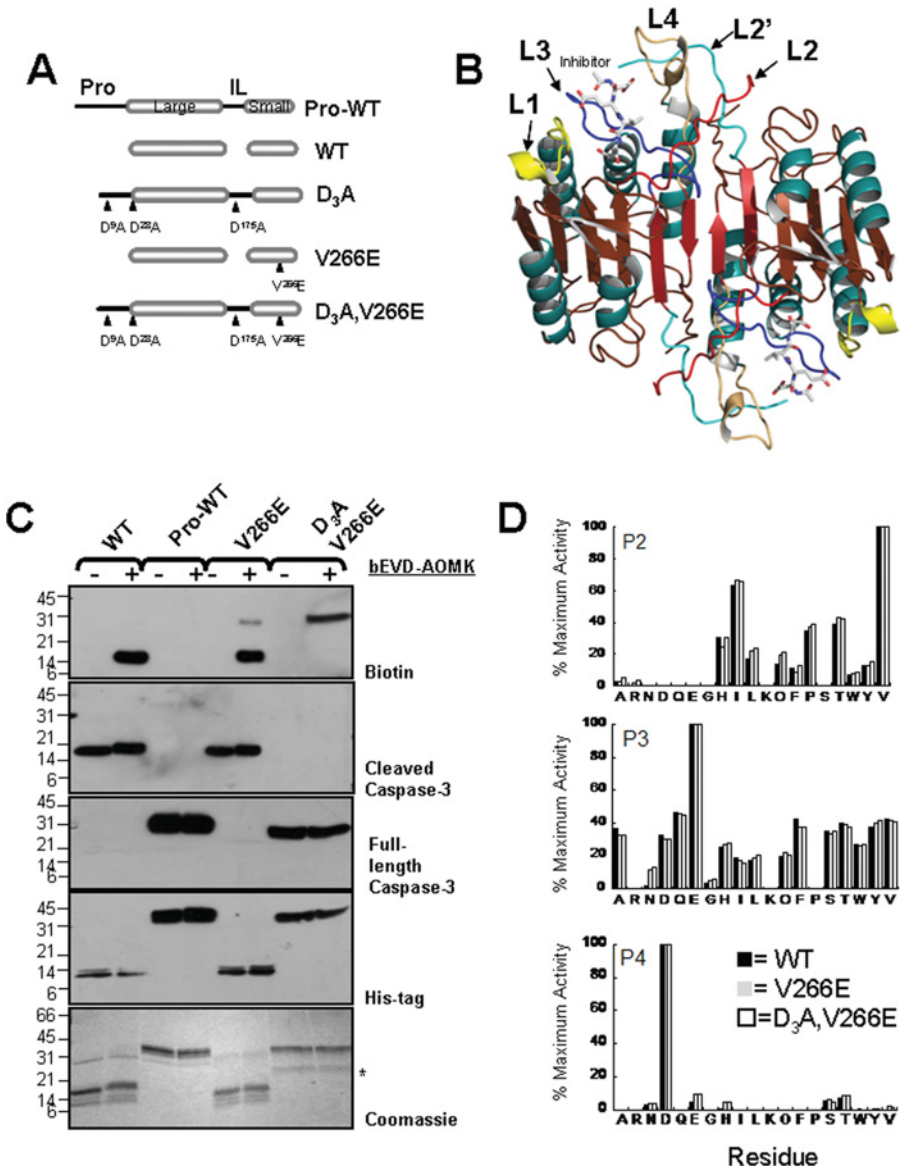

Figure 1 Procaspase-3(D_3A,V266E) is enzymatically active without cleavage of the IL

(**A**) The interface mutation V266E was designed in the context of wild-type caspase-3 (WT) and the uncleavable procaspase-3(D9A,D28A,D175A), called D_3A. Low expression generates 'one-chain' procaspase-3 (Pro-WT). Overexpression generates the 'two-chain' caspase-3 (WT or V266E) by automaturation. 'Pro' refers to the pro-domain. (**B**) Structure of WT caspase-3 (PDB code 2J30) highlighting the active site loops L1 (yellow), L2 (red), L3 (blue), L4 (brown) and L2′ (cyan). The prime (′) indicates residues from the second monomer. For clarity, only one active site is labelled. (**C**) Labelling the V266E mutants by affinity-based probes. Proteins labelled with bEVD-AOMK were probed by Western blot analysis with anti-biotin, anti-cleaved caspase-3, anti-full-length caspase-3 or anti-His-tag antibodies, or subjected to trichloroacetic acid precipitation and stained with Coomassie Blue. The positive control was WT, and the negative control was Pro-WT. The asterisk indicates a contaminating protein from *E. coli* expression. Molecular masses are shown to the left in kDa. (**D**) Determining the substrate specificity of the recombinant caspase-3 mutants. Activity of the caspase-3 mutants (10 nM) was measured using a tetrapeptide positional scanning library, with P1 fixed as an aspartate residue and 7-amino-4-carbamoylmethylcoumarin as the fluorophore group. Hydrolysis rates are presented as a percentage of the maximum rate for each subset (P2, P3 and P4).

bind to the interface of procaspase-3, resulting in its activation, may be a viable alternative to current therapies.

EXPERIMENTAL

Materials

Ac-DEVD-AFC (acetyl-Asp-Glu-Val-Asp-7-amino-4-trifluoromethylcoumarin) was prepared in the Salvesen laboratory, bEVD-AOMK (biotinylhexanoyl-Asp-Glu-Val-acyloxymethane; KMB01) was generously provided by Dr Matthew Bogyo (Stanford Comprehensive Cancer Center, Stanford, CA, U.S.A.), Z-VAD-FMK (benzyloxycarbonyl-Val-Ala-Asp-fluoromethyl ketone) was from Enzyme System Products, and Ac-DEVD-CMK (acetyl-Asp-Glu-Val-Asp-chloromethyl ketone) was from Calbiochem. Isopropyl β-D-thiogalactoside was from BioVectra.

Constructs

Plasmids expressing C-terminal His-tagged proteins (Figure 1A) have been described previously [11]. The following (pro)caspase-3 mutants were cloned into pcDNA3 (Invitrogen) as C-terminus FLAG-tag constructs: wild-type procaspase-3,

procaspase-3(D9A,D28A,D175A), procaspase-3(V266E) and procaspase-3(D9A,D28A,D175A,V266E). These constructs are referred to as WT, D_3A, V266E and 'D_3A,V266E' respectively. pcDNA3 containing the gene for Bax and pcDNA/myc-XIAP (X-linked inhibitor of apoptosis) were gifts from Dr John Reed (The Burnham Institute for Medical Research, La Jolla, CA, U.S.A.). C-terminal His-tagged caspase-3 mutants were expressed and purified as described previously [11]. Full-length XIAP (N-terminal His tag) [17] and baculovirus protein p35 [18] were expressed and purified as described previously.

Labelling with affinity-based probes

Proteins were diluted in buffer [50 mM Hepes, pH 7.8, 100 mM NaCl and 1 mM DTT (dithiothreitol)] at 250 nM final concentration and incubated with bEVD-AOMK (2.5 μM) for 30 min at room temperature ($\sim$25 °C) in a total volume of 500 μl. Half the samples were immediately subjected to Western blot analysis, and the other half were concentrated ten times by precipitation with trichloroacetic acid (10 %) and examined by SDS/PAGE (8–18 % gradient gel), followed by Coomassie Blue staining.

Positional scanning libraries

Positional scanning substrate combinatorial libraries (P4, P3 and P2 positions) were synthesized similarly to the previously published methods [19–21], as summarized in the Supplementary online data (at http://www.BiochemJ.org/bj/424/bj4240335add.htm).

Cell culture and transfection

HEK-293A (human embryonic kidney-293A) cells were cultivated in Dulbecco's modified Eagle's medium. Jurkat and MCF-7 cells were cultivated in RPMI 1640 medium. The media were supplemented with 10 % heat-inactivated bovine serum (Irvine Scientific), 2 mM L-glutamine and penicillin/streptomycin (Invitrogen). For transfection, the adherent cells, at 40–60 % confluence, were grown either in 6- or 12-well plates and were transfected using GeneJuice® (Novagen), as suggested by the manufacturer, with 3 μl of transfectant reagent per 1.0–2.0 μg of total DNA in 0.1 ml of serum-free medium. The control or the dilution vector for transfected DNA was pcDNA3. At 2 h post-transfection, Z-VAD-FMK (100 μM) or DMSO was added to the cultured cells. The final concentration of DMSO was 0.2 %. Cells were treated and harvested after 12–24 h, as described in the Figure legends. For flow cytometry experiments, cells were trypsinized on the plate, resuspended in the culture medium, washed with PBS and stained with Annexin V-PE using the Apoptosis Detection Kit (BioVision). Positive Annexin V-PE cells were analysed by FACS on a Becton Dickinson FACSort. Individual experiments were normalized by dividing each sample by the highest value (by Annexin V-PE staining) and multiplying by 100 to give 'percentage maximum apoptosis'. Statistical analysis was performed using the paired Student's *t* test with two-tailed distribution. Untreated duplicate samples were processed for immunoblotting and caspase activity assays. Preparation of cell lysates and caspase activity measurements were performed as summarized in the Supplementary online data.

Western blot analysis and antisera

Cell lysates, balanced for total protein concentration, were examined by SDS/PAGE (8–18 % polyacrylamide gradient gel). Proteins were transferred on to a PVDF membrane, blocked with 5 % (v/v) non-fat dried skimmed milk powder in TBS-T (20 mM Tris/HCl, pH 7.4, 150 mM NaCl and 0.1 % Tween 20) and subjected to immunoblotting overnight at 4 °C against the primary antibodies [in TBS-T with 5 % (v/v) non-fat dried skimmed milk powder]. The blot was washed with TBS-T followed by incubation for 1 h with the appropriate secondary antibody (1:10000) dissolved in TBS-T. The detection was performed using the femtomolar enhanced chemiluminessence kit from Pharmacia. The primary antibodies were used at the following dilutions: anti-FLAG (M2) 1:2000 (Sigma F3165); anti-PARP [poly(ADP-ribose) polymerase] 1:3000 (Pharmingen 556362); anti-cleaved PARP 1:1000 (Cell Signaling Technology #9541); anti-cleaved caspase-3 1:10000 (Cell Signaling Technology #9661); anti-full-length caspase-3 1:5000 (BD Transduction Laboratories clone 19); anti-ICAD 1:6000 (Cell Sciences PX024 and PX023); anti-Hsp-90 1:5000, anti-XIAP 1:2000 (BD Transduction Laboratories); and anti-His 1:1000 (Qiagen 34660). For biotin detection, the blots were blocked in 2 % (w/v) BSA (in TBS-T) overnight at 4 °C, then avidin–horseradish peroxidase (e-Bioscience; 18-4100-51) was added at 1:5000 dilution for 30 min at room temperature. Blots were washed three times for 10 min with TBS-T prior to ECL detection.

Crystallization and data collection

Crystals of caspase-3(V266E) were grown, and results were collected as described previously [22], except that the cryoprotectant consisted of 90 % reservoir buffer and 10 % 2-methyl-2,4-pentanediol (Hampton Research). Crystals were grown in the presence of the Ac-DEVD-CMK inhibitor and appeared within 4 days. A full data set was collected to a resolution of 1.63 Å (1 Å = 0.1 nm) at 100 K at the SER-CAT beamline (Advanced Photon Source, Argonne, IL, U.S.A.). V266E crystallized with the symmetry of the orthorhombic space group I222 with one heterodimer in the asymmetric unit. The biological dimer of heterodimers is generated through a 2-fold symmetry axis. The structure of V266E was determined using molecular replacement with the previously determined structure of caspase-3 for initial phasing (PDB entry 2J30). The inhibitor and all water molecules were removed from the initial model and all B-factors for protein atoms were set to 20 A^3. Inhibitor and water molecules were added in subsequent rounds of refinement performed with COOT [23] and CNS [24] and were positioned based on $2F_o - F_c$ and $F_o - F_c$ electron density maps contoured at the 1σ and 3σ levels respectively. Crystallographic data collection and refinement statistics are shown in Supplementary Table S1 (http://www.BiochemJ.org/bj/424/bj4240335add.htm). Procaspase-3 homology models were generated as summarized in the Supplementary online data. The atomic co-ordinates and structure factors for caspase-3(V266E) have been deposited in the PDB under accession code 3ITN.

RESULTS

Caspase-3(V266E) interface mutants are active before processing

The enzyme activity of D_3A,V266E was determined previously from the hydrolysis of a typical caspase fluorogenic substrate, Ac-DEVD-AFC [11]. In those studies, Western blot analysis showed that the high enzyme activity of D_3A,V266E could not be explained by an alternately cleaved protein because the enzyme activity was only $\sim$3–4-fold lower than that of the mature caspase-3. We examined this further by reacting the mutants with an active site probe developed for caspases, bEVD-AOMK, which labels the catalytic cysteine contained in a competent

active site. As shown in Figure 1(C, top panel), the probe covalently labelled the large subunit of WT (positive control), but not the intact single-chain wild-type procaspase-3 (negative control). Importantly, single-chain (uncleaved) D_3A,V266E was labelled nearly as well as the large subunit of cleaved V266E and WT. Because D_3A,V266E was shown previously to have enzymatic activity equal to that of the mature V266E [11], these results clearly show that the V266E mutation allows for activity of single chain caspase-3 in the absence of cleavage in the IL, at least on small synthetic substrates. Furthermore, the V266E mutation does not change the oligomeric properties of caspase-3 from high micromolar to picomolar range of protein concentration (see Supplementary Figure S1 at http://www.BiochemJ.org/bj/424/bj4240335add.htm) [11].

In order to determine whether the mutation changed the substrate specificity of the enzyme, we tested the P_2–P_4 sites in the V266E mutants using a positional scanning peptide library containing an aspartate residue fixed in the P_1 position (Figure 1D). The results show that there are no substantial differences between the specificity of WT and the V266E mutants for the P_2–P_4 positions, where maximum activity was obtained for the tetrapeptide sequence DEVD. Overall, the results show that the substrate specificities of the V266E mutants are very similar to that of wild-type caspase-3, and suggest that the active site of the activated procaspase resembles that of the mature caspase.

V266E interface mutants kill mammalian cells more efficiently than wild-type caspase-3

One predicts that expression of a constitutively active procaspase-3 should kill cells efficiently; indeed this has been shown previously for a circular permutation of the caspase that mimics IL cleavage [25]. However, it was not clear whether the ~ 3–4-fold lower activity of the V266E mutants compared with fully active wild-type caspase-3 represented sufficient activity for cell death. To examine this, we transiently transfected HEK-293A cells with various caspase-3 mutants and monitored cell viability by Annexin V staining (Figure 2A). Interestingly, both V266E and D_3A,V266E mutants resulted in robust cell death (~ 50 %), which exceeded that produced by WT and D_3A (~ 20 %). The loss in cell viability produced by the interface mutants was as pronounced as that produced by Bax, a cytotoxic protein that initiates the intrinsic apoptotic pathway at the mitochondrial level (Figure 2A). In all cases, the levels of apoptosis were decreased in the presence of a caspase inhibitor, Z-VAD-FMK, suggesting that the increased levels of cell death were dependent on caspase activity. When protein production was monitored by Western blot analysis, only the WT and D_3A species were detected by their reactivity to anti-FLAG antibodies (Figure 2B). Compared with the endogenous protein, the levels of WT were approx. 5–10-fold higher in transfected cells, as judged by the anti-caspase-3 immunoblot. The interface mutants could not be detected even after prolonged exposures of the FLAG immunoblots, after immunoblotting with anti-cleaved caspase-3 antibodies or when the proteasome inhibitor MG132 was added (results not shown). Thus the full-length procaspase-3 observed in the cells transfected with the interface mutants (Figure 2B, top panel) represents the endogenous protein. Immunoblots using cell lysates prepared at earlier time points post-transfection gave the same results (results not shown). However, RT–PCR (reverse transcription–PCR) reactions showed the presence of mRNA for the caspase variants (Supplementary Figure S2 at http://www.BiochemJ.org/bj/424/bj4240335add.htm), demonstrating that the genes were transcribed. The parsimonious explanation for the lack of immunostaining of transfected V266E

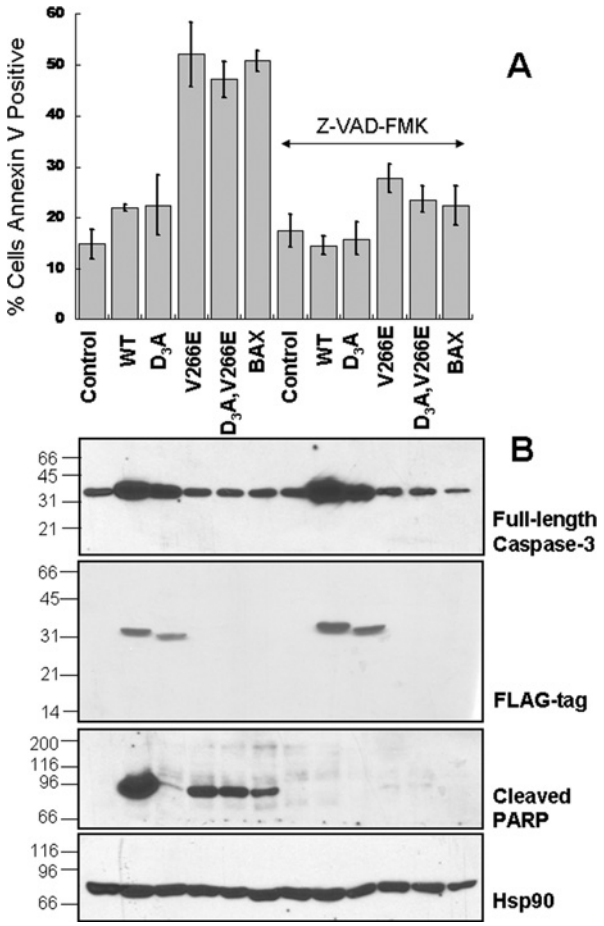

Figure 2 V266E mutants kill cells more efficiently than does the wild-type caspase-3

(**A**) HEK-293A cells were transiently transfected with FLAG-tagged caspase-3 DNA (or 50 ng Bax/0.95 μg empty vector), and Annexin V-positive cells were quantified after 24 h. Z-VAD-FMK (100 μM) or DMSO was added to the cultures 2 h post-transfection. The values represent the means for three independent experiments ± S.D. (**B**) Western blots of the cellular lysates from (**A**) against anti-full-length caspase-3 or anti-FLAG antibodies, for detection of the transfected constructs, or anti-cleaved PARP. The lower panel shows the loading control of Hsp90.

variants is that cells expressing them die before sufficient protein can accumulate, suggesting a lethal nature of the interface mutation. In support of this assertion, we replaced the catalytic cysteine residue in the V266E variants with a serine residue to remove activity. We find that the inactive V266E variants no longer support apoptosis (Supplementary Figure S3A at http://www.BiochemJ.org/bj/424/bj4240335add.htm). In addition, the proteins are observed by anti-FLAG antibody staining, although the accumulation remains lower than that for WT. These data show that the toxicity of the V266E variants requires catalytic activity.

In order to show that the cell death mediated by the interface mutants involved typical caspase substrates, we examined the cleavage of the canonical substrate PARP (Figure 2B). Cleaved PARP exits the nucleus and resides in the cytosol, so we examined the presence of cleaved PARP in mRIPA (for composition see the Supplementary Experimental section)-soluble lysates. As expected, PARP was cleaved in all cells displaying high Annexin V staining, and its cleavage was suppressed by Z-VAD-FMK (Figure 2B). Cleaved PARP appeared to be in higher amounts in cells transfected with WT, which may indicate a higher degradation rate of cleaved

PARP in cells transfected with the interface mutants or with Bax. We note that this experiment does not intend to quantify the amount of apoptosis, because the lysates were from cells collapsed in very late apoptosis, during which the process of protein degradation was advanced. The results in Figure 2(B) show the amount of cytosolic-cleaved PARP that leaked out of the nucleus at the specified time and had not been degraded yet by the proteasome. Owing to the fact that cells transfected with WT undergo very incipient apoptosis with no cleaved PARP degradation, the amount of cleaved PARP may seem higher in these cells in comparison with the cells transfected with V266E variants. However, in reality most of the PARP in the nucleus remained intact in cells transfected with WT, but was completely cleaved and removed from the nucleus in the V266E lysates. In addition, the cytosolic levels of cleaved PARP were much lower in the catalytically inactive C163S,V266E variants (Supplementary Figure S3B).

Overall, the results show that the constitutively active caspase-3 interface mutants were more efficient in killing transfected cells in culture than was wild-type caspase-3. Furthermore, the apoptotic activity of the V266E variants did not depend on the endogenous pool of procaspase-3. We transfected MCF7 cells, which lack endogenous caspase-3 [26], with plasmids containing the interface mutants, and we measured apoptosis by Annexin V staining (Supplementary Figure S4A at http://www.BiochemJ.org/bj/424/bj4240335add.htm). Although the transfection efficiency was lower than in the case of HEK-293A cells ($\sim 35\,\%$ compared with $\sim 60\,\%$ respectively), the pattern of cell death observed in the HEK-293A cells (Figure 2A) was reproduced in the MCF7 cells. One should note that Bax, the positive control, was less toxic in MCF7 cells than were the interface mutants due to the lack of endogenous caspase-3, the main effector caspase. In all cases, the number of apoptotic cells diminished in the presence of the caspase inhibitor Z-VAD-FMK.

Similarly, we could show that recombinant V266E cleaved caspase substrates in the absence of caspase-3 when added to crude cellular extracts. We examined hypotonic lysates from Jurkat cells that were immunodepleted of the endogenous caspase-3 and reconstituted with recombinant caspase-3 proteins. The lysates were analysed by Western blotting for cleavage of ICAD (Supplementary Figure S4B). We observed that ICAD was cleaved efficiently by the active WT and V266E proteins, and it remained unprocessed upon addition of the less active procaspase-3. The cleavage of ICAD was judged by the disappearance of the full-length protein for which the antibodies were developed.

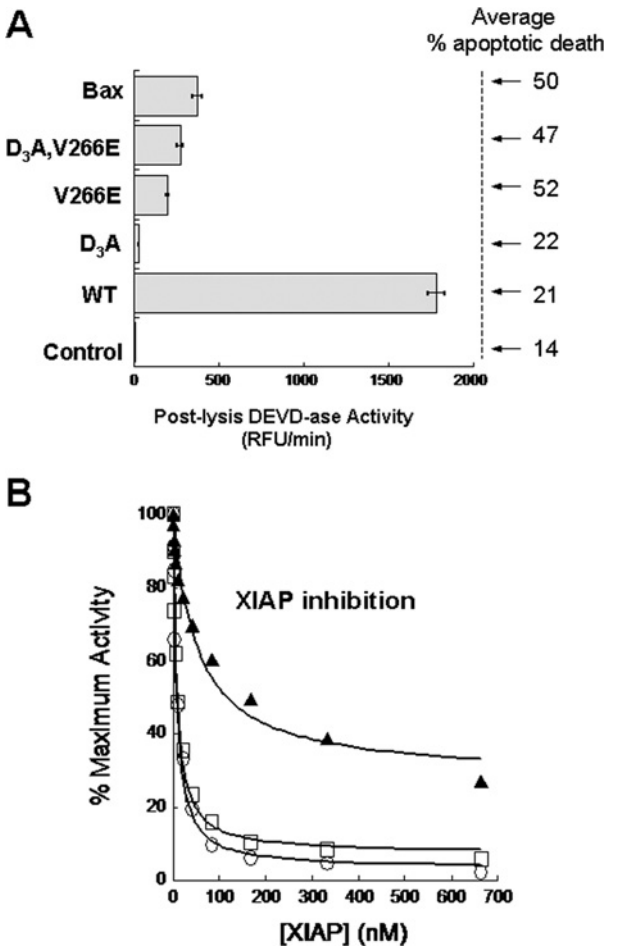

Figure 3 Wild-type caspase-3 lysates display higher DEVD-ase activity than those of V266E interface mutants

(**A**) Lysates from cells transfected for 24 h with the indicated plasmids were assayed for enzymatic activity. The values represent the means ± S.D. for three independent experiments. Values for the mean percentage apoptotic death are from Figure 2(A). RFU, relative fluorescence units. (**B**) Caspase-3 mutants (300 pM) were incubated with XIAP at the indicated concentration in XIAP assay buffer (see Supplementary Experimental section) for 30 min at 37 °C, and the remaining activity was tested against Ac-DEVD-AFC (100 μM). The activity rates were plotted as the percentage of the maximum velocity in the absence of the inhibitor. The data were fitted to an equation describing the enzymatic activity in the presence of a reversible competitive inhibitor (see Supplementary Experimental section), and results of the fits are shown in Table 1.

The intrinsic activity of interface mutants in transfected cells is lower than that of WT

We examined the threshold of caspase activity necessary to produce cell death by correlating the amount of death in cell culture with the total caspase activity in the corresponding lysates. We used the tetrapeptide substrate Ac-DEVD-AFC, which is cleaved primarily by effector caspases, to measure caspase activity in HEK-293A lysates that had been prepared from cells transfected with the interface mutants (same lysates as in Figure 2). Surprisingly, the lysates containing WT showed the highest DEVD-ase activity (Figure 3A). We expected to correlate this high activity to a high percentage of cell death in culture (see Figure 2A), which was not the case. In contrast, the lysates containing transfected interface mutants or Bax displayed less than 15 % of the DEVD-ase activity of the WT lysates (Figure 3A), despite the high amounts of Annexin V-positive cells present in the cell culture (Figure 2A). Lysates prepared from cells transfected with WT displayed high DEVD-ase activity as early as 12 h post-transfection, and the activity increased over time (Supplementary Figure S5A at http://www.BiochemJ.org/bj/424/bj4240335add.htm). However, lysates prepared from cells transfected with V266E showed modest DEVD-ase activity compared with WT for each time considered, and the activity did not peak earlier than 24 h (Supplementary Figure S5A). Because the rate of cell death peaked as early as 16 h after transfection with V266E (results not shown), the results suggest that the apoptotic cells may have leaked the cytosolic caspase-3 [27]. In that case, DEVD-ase activity should be observed in the cell culture medium. However, when we measured caspase activity in the supernatant after removing the cells by centrifugation, we found that indeed there was DEVD-ase activity in the cellular medium (Supplementary Figure S5B), but the ratio between the activity of V266E mutants and the activity of WT reflected the ratio found in the lysates (Figure 3A). Therefore, the 'missing' DEVD-ase activity was not in the cellular medium.

Table 1 XIAP inhibition constants for caspase-3 interface mutants

Caspase-3 protein	IC_{50} (nM)	K_i (nM)	Maximum inhibition (%)
WT	7.4 ± 0.8	1.75 ± 0.25	97 ± 2
V266E	7.6 ± 0.5	1.88 ± 0.11	93 ± 1.2
D_3A,V266E	51.4 ± 11.5	13.4 ± 2.6	72 ± 4.6

XIAP is a poor inhibitor of D_3A,V266E

The high DEVD-ase activity of caspase-3 in transfected cell lysates (Figure 3A) did not result in robust cell death (Figure 2A). It has been shown that cell death involves a XIAP-dependent threshold for activation of the effector caspases [28], where XIAP is an endogenous potent inhibitor of activated caspase-3 [29]. Our results suggest that caspase-3 could be inhibited in the cell by XIAP and that the mRIPA buffer (lysate preparation) and subsequent dilution into caspase assay buffer released XIAP from the active caspase-3, making measurement of the DEVD-ase activity possible. XIAP binds and inhibits cleaved caspase-3 via a two-step binding mechanism involving interactions with the active site and with the neo-epitope of the cleaved small subunit in L2′ [17]. Our data suggest that V266E becomes enzymatically active upon translation, without IL cleavage, so one predicts that XIAP will be a less potent inhibitor of the uncleaved procaspase D_3A,V266E, since one binding site (L2′) may not be accessible to XIAP. In order to test this hypothesis, we performed inhibition studies using recombinant WT and V266E interface mutants (Figure 3B and Supplementary Figure S6 at http://www.BiochemJ.org/bj/424/bj4240335add.htm). The results show that XIAP efficiently inhibited WT and V266E, presumably due to the fact that both proteins are cleaved (see Figure 1B). The IC_{50} and the K_i values for the cleaved proteins were similar (Table 1) and close to the values reported previously [17]. In contrast, D_3A,V266E was inhibited less efficiently by XIAP (Figure 3B), displaying a K_i value of ~ 8-fold higher in comparison with WT (Table 1). The results also showed that D_3A,V266E could be inhibited by XIAP only up to ~ 70 % of its maximum activity, compared with ~ 97 % for WT (Table 1). This information, translated to the intracellular environment where the XIAP concentration does not exceed 50–70 nM [28], suggests that the uncleaved mutant will be mostly uninhibited in the cell. Because Asp^{175} in the IL of procaspase-3 is a poor substrate for cleavage by mature caspase-3 [30,31], we suggest that the V266E mutants remain unprocessed in the cell at low concentrations, effectively avoiding inhibition by XIAP. This explains the early and robust cell death upon transfection with caspase-3 interface mutants in comparison with WT. We have ensured that the active sites of the interface mutants were equally competent for binding other inhibitors that did not require interaction with the cleaved form of caspase-3. For example, we show that the interface mutants were inhibited by baculovirus p35 (Supplementary Figure S6C) similarly to wild-type caspase-3. Furthermore, we performed co-transfection experiments with plasmids encoding the interface mutants and XIAP (Supplementary Figure S7 at http://www.BiochemJ.org/bj/424/bj4240335add.htm). We observed that XIAP inhibited cell death only when present in large excess compared with the caspase plasmid (>5:1 XIAP/caspase). Our results are consistent with a low concentration of activated procaspase-3 carrying out apoptosis. This assertion is consistent with concentrations of active caspase-3 determined by molecular simulation (1 nM) in the absence of XIAP and proteasome degradation [32].

The X-ray crystal structure of V266E

In order to examine structural changes caused by the replacement of Val^{266}, we crystallized and determined the structure of cleaved V266E to 1.63 Å (Supplementary Table S1). The motivation for replacing Val^{266} with a glutamate residue was prompted by the hydrophilic dimer interface of caspase-1, which contains Glu^{390} (equivalent to Val^{266} in caspase-3) and Arg^{391}. Glu^{390} forms a salt bridge with Arg^{286} (Arg^{164} in caspase-3), which is on L2, neutralizes the positive charge from that residue and appears to stabilize the active site.

Although the results show that the structure of V266E is very similar to that of WT (PDB code 2J30), with an overall RMSD (root mean square deviation) of 0.14 Å, two regions of the protein are different. Changes in one or both regions presumably result in the 3–4-fold lower enzyme activity. The first is derived from the IL, which in the uncleaved procaspase-3 is made of residues 169–190. Upon cleavage at Asp^{175} during maturation, residues 169–175 form L2 in the active site of one heterodimer and residues 176–190 reach across to the other heterodimer to form the active site L2′. L2′ is partially disordered in V266E, where we observe little or no electron density for amino acids 176–185. This is in contrast with the structure of WT, where the disorder is from residues 176–179. In WT, several residues in L2′ form a H-bonding network through water molecules with the P4 aspartate of the substrate (Figure 4A) [22], and the removal of these interactions was shown to decrease activity [33]. In V266E, we observe electron density starting with Lys^{186}. Importantly, $His^{185'}$ in WT forms two H-bonds with Thr^{245} at the C-terminus of helix 5. The contacts across the interface anchor the base of L4 with L2′, and these interactions are not observed in the mutant. Disruption of contacts at the C-terminus of helix 5 was shown previously to decrease the activity of procaspase-3 [34].

Secondly, the dimer interface of V266E has features in common with wild-type caspase-3 and with caspase-1, although Glu^{266} in the caspase-3 variant utilizes a different rotamer than does Glu^{390} in caspase-1. In this case, Glu^{266} interacts with Arg^{164} through a conserved water molecule (see Supplementary online data) rather than through direct interactions as observed in caspase-1 (Figures 4B and 4C). Interestingly, when Glu^{390} is replaced with an aspartate residue in caspase-1, the salt bridge with Arg^{286} is preserved but is mediated by a water molecule [9]. In WT, the positive charge of Arg^{164} is neutralized by Glu^{124}, and these contacts are maintained in the mutant (Figure 4B). When the structure is superimposed with that of caspase-1, one finds that only one of the two active sites aligns well (Figure 4C). When we modelled V266E with the same rotamer as that of caspase-1, we found steric clashes between Glu^{266} and $Glu^{266'}$, across the dimer interface, and between Glu^{266} and Tyr^{197}, on the adjacent β-strand (Figure 4D). This issue is alleviated in caspase-1 because of the presence of an insertion in β-strand 8, Arg^{391}, which allows Glu^{390} to adopt a rotamer that moves the carboxylate closer to Arg^{286} so that the two side chains are within H-bonding distance (2.8 Å), and because a cysteine residue (Cys^{331}) is present at the position equivalent to Tyr^{197} in WT. So, the rotamer adopted for Glu^{266} in the caspase-3 mutant seems to be somewhat of a compromise between avoiding steric clashes with neighbouring amino acids and optimizing favourable interactions with neighbouring residues and nearby water molecules.

Models of (in)active procaspase-3

Our previous biochemical data for D_3A,V266E [11], as well as that provided in the present study, show that the V266E mutation effectively shifts the zymogen to an active conformer. Currently there are no structures for procaspase-3, so we generated

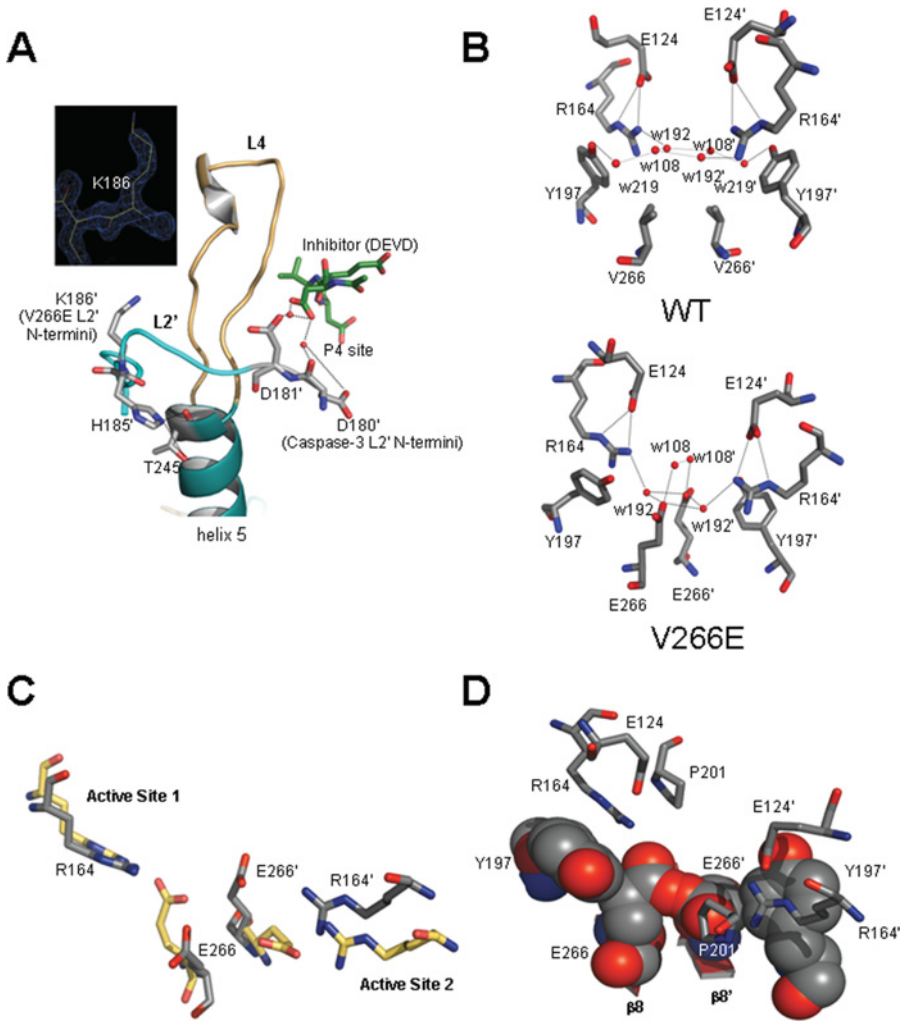

Figure 4 V266E changes the dimer interface

(**A**) Interactions in L2′ (cyan) with L4 (brown) and the P4-binding site of WT. Inset: N-termini of L2′ for V266E begins at Lys[186]. (**B**) Dimer interface of WT (upper panel) demonstrating neutralization of the positive charge of Arg[164] and six conserved water molecules (see Supplementary online data), and dimer interface of V266E (lower panel). Contacts between Glu[124] and Arg[164] are maintained in V266E, but two water molecules are removed and two are displaced by the carboxylate of Glu[266]. (**C**) Comparison of the dimer interface of V266E (grey) with that of caspase-1 (yellow). The rotamer at Glu[390] in caspase-1 allows closer contact with the active site arginine. (**D**) V266E modelled using the rotamer found in caspase-1 demonstrates intra- and inter-subunit steric clashes with Tyr[197] and Glu[266′].

homology models of the putative active and inactive zymogen in order to examine the conformational switch. Owing to their high sequence identity, we modelled inactive WT after procaspase-7 [35,36], and energy minimized the structures as described in the Experimental section (and the Supplementary online data) to assure that our final model is energetically feasible. We find that, similar to procaspase-7, the active sites in our model of the inactive zymogen are disorganized and the IL occupies the central cavity. There are two monomers, represented by chains A and B, forming a complete dimer in the asymmetric unit of the procaspase-7 X-ray crystal structure. Our model of the inactive procaspase-3 is similar to the entire dimer. Although the IL from chain A (IL-A) in the procaspase-7 template mostly remains exposed to solvent, a large portion of IL-B is buried in the interface, making contacts with several interface residues and shielding the hydrophobic core from water (Figure 5A).

An examination of the model for inactive procaspase-3 shows two features of the protein that may be involved in maintaining the inactive conformer. First, the dimer is asymmetric due to the binding of residues Val[178]–Glu[190] from IL-B in the interface. As a result of the binding of IL-B, only residues His[185]–Glu[190] from IL-A are observed near the interface, and these residues mostly interact with active site B. The asymmetric binding of the two ILs leads to inhibition of the two active sites (from chains A and B) in two complementary manners. For active site A, residues Cys[184]–Val[189] from IL-B prevent insertion of active site loop 3 (chain A) into the dimer interface (Figure 5B). Cys[184] and Val[189] (IL-B) in the inactive procaspase-3 reside in the region occupied by Pro[201] (chain A) in the active caspase-3. A similar sequence in caspase-7 was referred to as the 'blocking segment' because the residues prevent formation of the substrate-binding pocket [35]. In addition, steric clashes between the side chain of His[185] (IL-B) and the backbone atoms of Gly[202] (L3) and Arg[164] (L2) (chain A) probably prevent rotation of L2 from chain A into the active conformation, where the side chain of Arg[164] rotates into the dimer interface to intercalate between Pro[201] and Tyr[197], and the catalytic Cys[163] rotates into the P1 site (see Figure 5B, grey model). Similar steric constraints are observed in procaspase-7 (Figure 5B, yellow

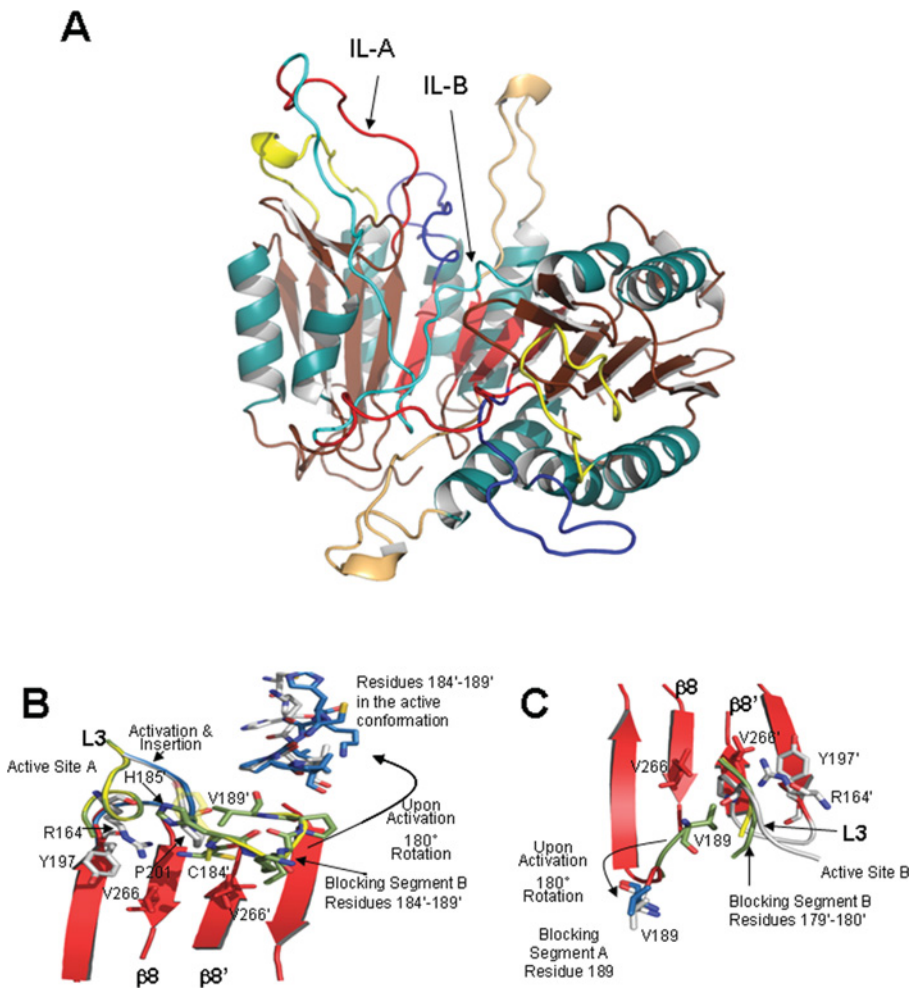

Figure 5 Homology models of (in)active procaspase-3

(**A**) Model of inactive procaspase-3 demonstrating binding of the IL (cyan) in the dimer interface, preventing organization of the active site loops. Colour code is the same as that used in Figure 1(B). Note that L2 and L2′ are covalently connected in the IL. (**B**) Superposition of inactive procaspase-3 (green residues) and of procaspase-7 (yellow) shows the blocking segment of IL-B, residues 184′–189′ (procaspase-3 numbering), prevents insertion of active site loop 3 from monomer A. For clarity, only one residue from the blocking segment of procaspase-7 is shown (semi-transparent sticks, Tyr^{211}), whereas all of the residues of the blocking segment of procaspase-3 are highlighted (green). Upon cleavage of the IL, L2′, where the blocking segment resides, rotates ∼ 180° and vacates the interface. Subsequently, a portion of the substrate-binding loop is permitted to insert in the interface. Arg^{164}, Tyr^{197} and Pro^{201} engage in a stacking interaction (shown as the white residues) once L3 inserts in the interface. Insertion of the substrate-binding loop is permitted in the active procaspase-3 (blue ribbon) as the blocking segment lifts out of the interface upon activation (blue residues). (**C**) Superposition of procaspase-7 (yellow) and of inactive procaspase-3 (green) reveals a blocking segment involving residues 179′–180′ (caspase-3 numbering) of IL-B and Val^{189} of IL-A, preventing insertion of L3 in the active site of monomer B. L3 (white ribbon, WT) cannot insert into the interface until the blocking segment (green, inactive procaspase-3; yellow, procaspase-7) vacates the interface.

model). In the active procaspase-3, as well as upon cleavage of the IL to yield caspase-3, removal of the blocking segment of IL-B from the interface allows Pro^{201} from chain A to move ∼ 6 Å into the active conformation, thus forming the substrate-binding pocket for active site A. For active site B, a blocking segment also prevents insertion of Pro^{201} and the substrate-binding pocket, but the interactions differ due to the asymmetric nature of the inactive procaspase-3 dimer (Figure 5C). In this case, Val^{189} (IL-A) resides in the region occupied by Pro^{201} (chain B) in the active caspase-3, so Val^{189} behaves similarly for both ILs. However, the remainder of the blocking segment is comprised of the backbone atoms of residues 179–182 from IL-B, which also reside in the region occupied by Pro^{201}-Tyr^{203} of the active caspase-3. Thus, although the mechanisms differ somewhat for each active site, the substrate-binding loops of both active sites are prevented from inserting into the interface because the interface is occupied by segments of IL-A and IL-B.

In addition to the blocking segments, a cluster of hydrophobic amino acid residues centred about Val^{266} appears to stabilize the inactive conformer (Figure 6A), and a substitution of a glutamate residue for Val^{266} in the model of the inactive procaspase-3 suggests a mechanism for activation resulting from the mutation. The hydrophobic cluster is comprised of seven residues: $Met^{182'}$, from IL-B, and Ile^{187}, $Ile^{187'}$, Val^{189}, $Val^{189'}$, Val^{266}, and $Val^{266'}$ from both monomers (Figure 6A). On the basis of this analysis, we suggest that V266E activates the procaspase by disrupting the hydrophobic cluster and introducing steric clashes with $Met^{182'}$ and $Ile^{187'}$ (Figure 6B), essentially expelling the IL from the dimer interface: the first and most important step in activation. Because the glutamate side chain is approx. 2.5 Å longer than that of valine, the IL is prevented from rebinding in the interface after its release, and the protein conformation shifts to the active state. It is important to note that the conformational shift occurs without cleavage of the polypeptide chain at Asp^{175}. In the

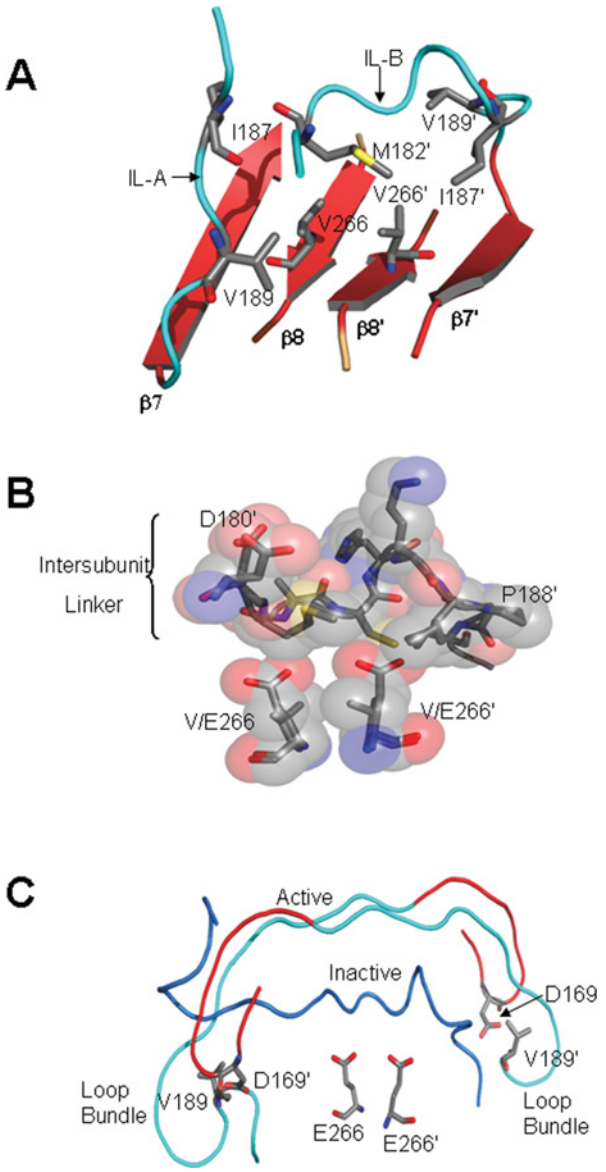

Figure 6 V266E expels the IL from the interface

(**A**) Hydrophobic cluster in the inactive procaspase-3 centred about Val[266]. Residues in the IL (cyan) of both monomers contribute to the cluster. (**B**) Because the glutamate side chain is longer than that of valine, the V266E mutation probably disrupts the hydrophobic cluster, preventing the IL from binding in the interface. (**C**) Comparison of the IL in the inactive and active procaspase-3. H-bonds contributed by the loop bundle, and centred about Asp[169], are critical to active site stabilization. These contacts form only in the active conformer.

active conformer, both ILs occupy a region above the central cavity, but have very few stabilizing contacts with the protease domain (Figure 6C). Ramachandran plots show that the backbone torsion angles are satisfactory (Supplementary Table S1), and energy minimization was performed in CHARMm [37] to alleviate energetically unfavourable conformations within the protein (see Supplementary Experimental section at http://www.BiochemJ.org/bj/424/bj4240335add.htm). Whether or not the conformational details are correct, the most important revelation obtained from our model of the active procaspase-3 (Figure 6C) is that the IL is indeed long enough to allow formation of the loop bundle at both active sites (contacts between Asp[169] and Val[189′]). Similar to caspase-7, removal of the blocking segment from the central cavity allows L3 to move into the dimer interface, Arg[164] to rotate out of the substrate-binding pocket and into the interface, and the catalytic groups to move into their active positions so that the active site is organized similarly to the mature caspase-3. Because L2 and L2′ remain covalently connected in the IL, however, putative stabilizing interactions provided by L2′ with the P4 aspartate of the substrate, described above, are not possible in the procaspase. Supplementary Movie S2 (at http://www.BiochemJ.org/bj/424/0335/bj4240335add.htm) shows the conformational switch between inactive and active procaspase-3.

DISCUSSION

We show that the variant (pro)caspase-3 kills mammalian cells rapidly compared with wild-type caspase-3. D_3A,V266E is active in the cell upon translation, and before processing at Asp[175], and cleaves substrates similarly to the mature caspase. These features are important for two reasons. First, endogenous procaspase-3 is a poor substrate for D_3A,V266E, so cell death occurs due to the activity of the procaspase variant on cellular substrates rather than its activation of endogenous procaspase-3. In support of this conclusion, we showed that MCF-7 cells, which lack procaspase-3, undergo apoptosis when transfected with D_3A,V266E. Secondly, inhibition of the mutant by XIAP is weak because the procaspase is not processed. In this case, the neo-epitope at the N-terminus of L2′, which serves as a second binding region for XIAP, remains sequestered in the procaspase.

The low threshold of activated procaspase-3 is much lower than the total cellular concentration of caspase-3, which is ~ 100 nM in apoptotic Jurkat [4] and HEK-293 cells [30]. The concentration of the zymogen appears to be higher than that of mature caspase-3 [38], although HeLa cells are estimated to contain approx. 120 nM procaspase-3 [28]. Under normal cellular conditions, XIAP concentrations of 50–60 nM [28] are sufficient to inhibit the small amount of activated caspase-3 and to target the protein for degradation by the proteasome [39]. The induction of apoptosis leads to massive activation of endogenous procaspase-3, which overwhelms the control system and results in rapid cell death [32]. Because XIAP does not efficiently inhibit D_3A,V266E, a low concentration of the pseudo-activated procaspase is sufficient for rapid cell death.

The interface mutation has little effect on the structure of the mature caspase, but it appears to have a larger effect on that of the procaspase. Our structural data show that L2′ is disordered in V266E, and conserved water molecules are displaced at the interface. At present, it is not clear how a mutation in the interface affects ordering of L2′, since the regions that are affected are >25 Å from the site of the mutation. Although residues in L2′ H-bond with the P4 carboxylate of the substrate, removal of those interactions do not significantly affect the enzymatic reaction. Val[266] resides at the centre of β-strand 8 in a water-filled cavity, with the closest water molecules approx. 3.5 Å from the hydrophobic side chains, well within van der Waals contacts. As described by Wells and co-workers, this region of the interface encompasses a site for binding of allosteric inhibitors, which prevent active site formation, in general, by preventing the insertion of the substrate-binding loop (L3) into the active site cavity [10]. This is important because part of L3 extends into the dimer interface and forms new contacts with residues in L2 in addition to forming the base of the substrate-binding pocket. The allosteric binding pocket is occluded in the procaspase due to the positioning of the IL in the interface, and the 'blocking segment' of the IL prevents insertion of L3 into the active site. Our results from the present study suggest that the inhibition is alleviated in

D_3A,V266E so that the IL is removed from the allosteric site, allowing the active site loops to organize. Thus the allosteric site linked to inhibition of the active caspase also stabilizes the inactive procaspase.

The inactive conformer appears to be stabilized by hydrophobic and charge–charge interactions across the dimer interface, and these stabilizing contacts are disrupted in the active conformer. Upon removal from the interface-binding site, the IL moves across the surface of the protein to form the critical contacts contributed by Asp^{169}, and the active conformer is stabilized primarily by backbone H-bonds between the two ILs and those that form at Asp^{169}. Stabilizing interactions in the mature caspase, contributed by L2, L2′, L3 and L4, are unable to form in the active procaspase. The lack of these stabilizing interactions may explain, in part, why the inactive procaspase-3 is favoured.

Learning to selectively manipulate the level of apoptosis is expected to lead to therapeutic strategies for a number of diseases in which the dysregulation of apoptosis is a common factor. Cancer cells, for example, typically have gained the ability to circumvent apoptosis, so the proteins in the apoptotic cascades have become ideal targets for cancer therapy [40–42]. We suggest that directly targeting procaspase-3 could lead to more effective therapy and lower drug resistance, since effector caspases are the terminal proteases in the cell death programme. Our results suggest that small molecules could bind to the dimer interface of the zymogen and effectively mimic the effects of the V266E mutation by releasing the IL from the allosteric site in the interface. One advantage of this strategy, as shown in the present study, is that the activation of endogenous procaspase-3 could occur without cleavage at Asp^{175} and may circumvent inhibition by XIAP. Thus, compounds that induce a conformational change in the zymogen, as does the V266E mutation, may show great potential in drug design strategies. Modulation of caspase inactivation from the dimer interface has been proposed before [10], but we are the first to show that the reverse mechanism, activation, is possible by manipulating the dimer interface.

AUTHOR CONTRIBUTION

A. Clay Clark and Guy Salvesen designed the study. Jad Walters, Paul Swartz, Carla Mattos and A. Clay Clark carried out crystallographic and modelling studies. Cristina Pop, Fiona Scott and Guy Salvesen carried out cell biological studies. Marcin Drag synthesized the peptide library. Jad Walters, Cristina Pop, Carla Mattos, Guy Salvesen and A. Clay Clark wrote the manuscript.

ACKNOWLEDGEMENTS

We thank the research agencies of North Carolina State University and the North Carolina Agricultural Research Service for continued technical support.

FUNDING

This work was supported by a grant from the NIH (National Institutes of Health) [grant number GM065970 (to A.C.C.)]. The crystallography and modelling work were supported by an NIH grant [grant number CA096867 (to C.M.)]. Use of the Advanced Photon Source was supported by the U.S. Department of Energy, Office of Science, Office of Basic Energy Sciences, under contract number W-31-109-ENG-38.

REFERENCES

1 Boatright, K. M. and Salvesen, G. S. (2003) Mechanisms of caspase activation. Curr. Opin. Cell Biol. **15**, 725–731
2 Renatus, M., Stennicke, H. R., Scott, F. L., Liddington, R. C. and Salvesen, G. S. (2001) Dimer formation drives the activation of the cell death protease caspase 9. Proc. Natl. Acad. Sci. U.S.A. **98**, 14250–14255
3 Pop, C., Fitzgerald, P., Green, D. R. and Salvesen, G. S. (2007) Role of proteolysis in caspase-8 activation and stabilization. Biochemistry **46**, 4398–4407
4 Pop, C., Chen, Y.-R., Smith, B., Bose, K., Bobay, B., Tripathy, A., Franzen, S. and Clark, A. C. (2001) Removal of the pro-domain does not affect the conformation of the procaspase-3 dimer. Biochemistry **40**, 14224–14235
5 Bose, K., Pop, C., Feeney, B. and Clark, A. C. (2003) An uncleavable procaspase-3 mutant has a lower catalytic efficiency but an active site similar to that of mature caspase-3. Biochemistry **42**, 12298–12310
6 MacKenzie, S. H. and Clark, A. C. (2008) Targeting cell death in tumors by activating caspases. Curr. Cancer Drug Targets **8**, 98–109
7 Fuentes-Prior, P. and Salvesen, G. S. (2004) The protein structures that shape caspase activity, specificity activation and inhibition. Biochem. J. **384**, 201–232
8 Shi, Y. (2004) Caspase activation, inhibition, and reactivation: a mechanistic view. Protein Sci. **13**, 1979–1987
9 Datta, D., Scheer, J. M., Romanowski, M. J. and Wells, J. A. (2008) An allosteric circuit in caspase-1. J. Mol. Biol. **381**, 1157–1167
10 Hardy, J. A., Lam, J., Nguyen, J. T., O'Brien, T. and Wells, J. A. (2004) Discovery of an allosteric site in the caspases. Proc. Natl. Acad. Sci. U.S.A. **101**, 12461–12466
11 Pop, C., Feeney, B., Tripathy, A. and Clark, A. C. (2003) Mutations in the procaspase-3 dimer interface affect the activity of the zymogen. Biochemistry **42**, 12311–12320
12 Reed, J. C. (2006) Proapoptotic multidomain Bcl-2/Bax-family proteins: mechanisms, physiological roles, and therapeutic opportunities. Cell Death Differ. **13**, 1378–1386
13 Diehl, V., Stein, H., Hummel, M., Zollinger, R. and Connors, J. M. (2003) Hodgkin's lymphoma: biology and treatment strategies for primary, refractory, and relapsed disease. Hematology **2003**, 225–247
14 Estrov, Z., Thall, P. F., Talpaz, M., Estey, E. H., Kantarjian, H. M., Andreeff, M., Harris, D., Van, Q., Walterscheid, M. and Kornblau, S. M. (1998) Caspase 2 and caspase 3 protein levels as predictors of survival in acute myelogenous leukemia. Blood **92**, 3090–3097
15 Krepela, E., Prochazka, J., Fiala, P., Zatloukal, P. and Selinger, P. (2006) Expression of apoptosome pathway-related transcripts in non-small cell lung cancer. J. Cancer Res. Clin. Oncol. **132**, 57–68
16 Grigoriev, M. Y., Pozharissky, K. M., Hanson, K. P., Imyanitov, E. N. and Zhivotovsky, B. (2002) Expression of caspase-3 and -7 does not correlate with the extent of apoptosis in primary breast carcinomas. Cell Cycle **1**, 337–342
17 Scott, F. L., Denault, J.-B., Riedl, S. J., Shin, H., Renatus, M. and Salvesen, G. S. (2005) XIAP inhibits caspase-3 and -7 using two binding sites: evolutionarily conserved mechanism of IAPs. EMBO J. **24**, 645–655
18 Riedl, S. J., Renatus, M., Snipas, S. J. and Salvesen, G. S. (2001) Mechanism-based inactivation of caspases by the apoptotic suppressor p35. Biochemistry **40**, 13274–13280
19 Thornberry, N. A., Rano, T. A., Peterson, E. P., Rasper, D. M., Timkey, T., Carcia-Calvo, M., Hotzager, V. M., Nordstrom, P. A., Roy, S., Vaillancourt, J. P. et al. (1997) A combinatorial approach defines specificities of members of the caspase family and granzyme B. J. Biol. Chem. **272**, 17907–17911
20 Harris, J. L., Backes, B. J., Leonetti, F., Mahrus, S., Ellman, J. A. and Craik, C. S. (2000) Rapid and general profiling of protease specificity by using combinatorial fluorogenic substrate libraries. Proc. Natl. Acad. Sci. U.S.A. **97**, 7754–7759
21 Drag, M., Mikolajczyk, J., Krishnakumar, I. M., Huang, Z. and Salvesen, G. S. (2008) Activity profiling of human deSUMOylating enzymes (SENPs) with synthetic substrates suggests an unexpected specificity of two newly characterized members of the family. Biochem. J. **409**, 461–469
22 Feeney, B., Pop, C., Swartz, P., Mattos, C. and Clark, A. C. (2006) Role of loop bundle hydrogen bonds in the maturation and activity of (pro)caspase-3. Biochemistry **45**, 13249–13263
23 Emsley, P. and Cowtan, K. (2004) COOT: model-building tools for molecular graphics. Acta Crystallogr. Sect. D Biol. Crystallogr. **60**, 2126–2132
24 Brunger, A. T., Adams, P. D., Clore, G. M., Delano, W. L., Gros, P., Grosse-Kunstleve, R. W., Jiang, J. S., Kuszewski, J., Nilges, M., Panni, N. S. et al. (1998) Crystallography and NMR system: a new software suite for macromolecular structure determination. Acta Crystallogr. Sect. D Biol. Crystallogr. **54**, 905–921
25 Srinivasula, S. M., Ahmad, M., MacFarlane, M., Luo, Z., Huang, Z., Fernandes-Alnemri, T. and Alnemri, E. S. (1998) Generation of constitutively active recombinant caspases-3 and -6 by rearrangement of their subunits. J. Biol. Chem. **273**, 10107–10111
26 Janicke, R. U., Sprengart, M. L., Wati, M. R. and Porter, A. G. (1998) Caspase-3 is required for DNA fragmentation and morphological changes associated with apoptosis. J. Biol. Chem. **273**, 9357–9360
27 Krysko, D. V., Vanden Berghe, T., D'Herde, K. and Vandenabeele, P. (2008) Apoptosis and necrosis: detection, discrimination and phagocytosis. Methods **44**, 205–221
28 Rehm, M., Huber, H. J., Dussmann, H. and Prehn, J. H. M. (2006) Systems analysis of effector caspase activation and its control by X-linked inhibitor of apoptosis protein. EMBO J. **25**, 4338–4349

29 Eckelman, B. P., Salvesen, G. S. and Scott, F. L. (2006) Human inhibitor of apoptosis proteins: why XIAP is the black sheep of the family. EMBO Rep. **7**, 988–994
30 Stennicke, H. R., Jurgensmeier, J. M., Shin, H., Deveraux, Q., Wolf, B. B., Yang, X., Zhou, Q., Ellerby, M., Ellerby, L. M., Bredesen, D. et al. (1998) Pro-caspase-3 is a major physiologic target of caspase-8. J. Biol. Chem. **273**, 27084–27090
31 Liu, H., Chang, D. W. and Yang, X. (2005) Interdimer processing and linearity of procaspase-3 activation. J. Biol. Chem. **280**, 11578–11582
32 Albeck, J. G., Burke, J. M., Aldridge, B. B., Zhang, M., Lauffenburger, D. A. and Sorger, P. K. (2008) Quantitative analysis of pathways controlling extrinsic apoptosis in single cells. Mol. Cell **30**, 11–25
33 Ganesan, R., Mittl, P. R. E., Jelakovic, S. and Grutter, M. G. (2006) Extended substrate recognition in caspase-3 revealed by high resolution X-ray structure analysis. J. Mol. Biol. **359**, 1378–1388
34 Feeney, B., Pop, C., Tripathy, A. and Clark, A. C. (2004) Ionic interactions near loop L4 are important for maintaining the active site environment and the dimer stability of (pro)caspase-3. Biochem. J. **384**, 515–525
35 Riedl, S. J., Fuentes-Prior, P., Renatus, M., Kairies, N., Krapp, S., Huber, R., Salvesen, G. S. and Bode, W. (2001) Structural basis for the activation of human procaspase-7. Proc. Natl. Acad. Sci. U.S.A. **98**, 14790–14795
36 Chai, J., Wu, Q., Shiozaki, E., Srinivasula, S. M., Alnemri, E. S. and Shi, Y. (2001) Crystal structure of a procaspase-7 zymogen: mechanisms of activation and substrate binding. Cell **107**, 399–407
37 Brooks, B. R., Bruccoleri, R. E., Olafson, B. D., States, D. J., Swaminathan, S. and Karplus, M. (1983) CHARMM: A program for macromolecular energy, minimization, and dynamics calculations. J. Comp. Chem. **4**, 187–217
38 Saunders, P. A., Cooper, J. A., Roodell, M. M., Schroeder, D. A., Borchert, C. J., Isaacson, A. L., Schendel, M. J., Godfrey, K. G., Cahill, D. R., Walz, A. M. et al. (2000) Quantification of active caspase 3 in apoptotic cells. Anal. Biochem. **284**, 114–124
39 Suzuki, Y., Nakabayashi, Y. and Takahashi, R. (2001) Ubiquitin-protein ligase activity of X-linked inhibitor of apoptosis protein promotes proteasomal degradation of caspase-3 and enhances its anti-apoptotic effect in Fas-induced cell death. Proc. Natl. Acad. Sci. U.S.A. **98**, 8662–8667
40 Vogelstein, B. and Kinzler, K. W. (2001) Achilles' heel of cancer? Nature **412**, 865–866
41 Kirkin, V., Joos, S. and Zornig, M. (2004) The role of Bcl-2 family members in tumorigenesis. Biochem. Biophys. Acta **1644**, 229–249
42 Soengas, M. S., Capodleci, P., Polsky, D., Mora, J., Esteller, M., Opitz-Araya, X., McComble, R., Herman, J. G., Gerald, W. L., Lazebnik, Y. A. et al. (2001) Inactivation of the apoptosis effector Apaf-1 in malignant melanoma. Nature **409**, 207–211

Received 29 May 2009/8 September 2009; accepted 30 September 2009
Published as BJ Immediate Publication 30 September 2009, doi:10.1042/BJ20090825

Biochem. J. (2009) **424**, 335–345 (Printed in Great Britain) doi:10.1042/BJ20090825

online data

SUPPLEMENTARY ONLINE DATA

A constitutively active and uninhibitable caspase-3 zymogen efficiently induces apoptosis

Jad WALTERS*, Cristina POP†, Fiona L. SCOTT†, Marcin DRAG†[1], Paul SWARTZ*, Carla MATTOS*, Guy S. SALVESEN† and A. Clay CLARK*[2]

*Department of Molecular and Structural Biochemistry, North Carolina State University, Raleigh, NC 27695, U.S.A., and †Program in Apoptosis and Cell Death, The Burnham Institute for Medical Research, 10901 N Torrey Pines Rd, La Jolla, CA 92037, U.S.A.

The interface mutants do not affect oligomerization

Although the V266E mutation does not change the oligomeric properties of caspase-3 at higher protein concentrations (micromolar range) [1], we examined whether the mutation weakens the dimer interface at lower protein concentrations by performing dilution experiments coupled with enzyme activity measurements (see Figure S1). The data follow a unimolecular mechanism, suggesting that, at least in the presence of the substrate, the caspase-3 mutants were stable dimers in the picomolar range of protein concentration.

The interface mutants kill cells independently of endogenous caspase-3

Because the substrate specificity is the same for the V266E variants and WT (see Figure 1D in the main text), it is likely that the mutants cleave the same substrates as caspase-3 during apoptosis. Alternatively, it is possible that the interface mutants activate the endogenous caspase-3, which then amplifies the downstream proteolytic events, although this is unlikely given that procaspase-3 is typically a poor substrate for active caspase-3 [2]. To examine the latter possibility, we transfected MCF7 cells, which lack endogenous caspase-3 [3], with plasmids containing the interface mutants, and we measured apoptosis by Annexin V staining (see Figure S4A). Although the transfection efficiency was lower than in the case of HEK-293A cells ($\sim 35\,\%$ compared with $\sim 60\,\%$ respectively), the pattern of cell death observed in the HEK-293A cells (see Figure 2A in the main text) was reproduced in the MCF7 cells (see Figure S4A). One should note that Bax, the positive control, was less toxic in MCF7 cells than were the interface mutants due to the lack of endogenous caspase-3, the main effector caspase. In all cases, the number of apoptotic cells diminished in the presence of the caspase inhibitor Z-VAD-FMK.

Similarly, recombinant V266E cleaved caspase substrates in the absence of caspase-3 when added to crude cellular extracts. We examined hypotonic lysates from Jurkat cells that were immunodepleted of the endogenous caspase-3 and reconstituted with recombinant caspase-3 proteins. The lysates were analysed by Western blot for cleavage of ICAD (see Figure S4B). We observed that ICAD was cleaved efficiently by the active WT and V266E proteins, and it remained unprocessed upon addition of the less active procaspase-3. The cleavage of ICAD was judged by the disappearance of the full-length protein for which the antibodies were developed. Lysate prepared from cells treated with Z-VAD-FMK showed no DEVD-ase activity (results not shown).

Conserved water molecules in the dimer interface

On one side of the interface, α-helices 5 and 5′ border β-strands 8 and 8′, whereas the opposite face has a water-filled cavity (see [4] for review). Moreover, several of the water molecules found in the central cavity are conserved. We examined over 5000 crystallographic water molecules in 20 caspase-3 structures with a resolution of 2.5 Å or better, including proteins from our own studies as well as those deposited in the PDB. We considered water molecules that were within 1.4 Å of one another to be conserved, using a previously published method [4a]. The structures included in our conserved water analysis were obtained from crystals with symmetry of various space groups formed under different crystallization conditions and differing in the number of molecules per asymmetric unit. Overall, the analysis identified several conserved water molecules throughout the structure of caspase-3, but we focus in the present study on six conserved hydration sites in the dimer interface, which are found in a pseudo-planar arrangement approx. 3.8 Å above the $Val^{266}/Val^{266'}$ side chains (see Figure 4B of the main text).

In WT, Wat219 (where Wat is a water molecule) and Wat219′ H-bond with the hydroxy groups of Tyr^{197} and $Tyr^{197'}$ respectively. Both of these water molecules also interact with four central crystallographic water molecules to provide a H-bonding network bridging the two active sites. Wat192 and Wat192′ in this network also H-bond to Arg^{164} and $Arg^{164'}$ respectively. The water network is disrupted in V266E, where Wat219 and Wat219′ are removed, and the four central water molecules move to prevent clashes with Glu^{266} (Figure 4B). Interestingly, the carboxylates of Glu^{266} and $Glu^{266'}$ displace Wat108 and Wat108′ respectively, and maintain the planar contacts with Wat192 and Wat192′. Overall, this arrangement preserves the H-bonding network between Arg^{164} and $Arg^{164'}$, but removes H-bonds contributed by Tyr^{197} and $Tyr^{197'}$.

EXPERIMENTAL

Positional scanning libraries

In the first step, Fmoc (fluoroen-9-ylmethoxycarbonyl)-ACC fluorophore was coupled to the Rink Amide Resin (Novabiochem) using a procedure described previously [5]. The Fmoc protecting group was removed using 20 % piperidine in DMF (dimethylformamide). Coupling of the Fmoc-Asp(O-tBut)-COOH was carried out in DMF using HATU as the coupling reagent and in the presence of the 2,4,6-collidine base for 24 h at room temperature. This step was repeated twice. The unreacted ACC was acetylated as described previously [5]. The Fmoc protecting

[1] Current address: Division of Medicinal Chemistry and Microbiology, Faculty of Chemistry, Wroclaw University of Technology, Wybrzeze Wyspianskiego 27, 50-370 Wroclaw, Poland

[2] To whom correspondence should be addressed (email clay_clark@ncsu.edu).

The atomic co-ordinates and structure factors for caspase-3(V266E) have been deposited in the PDB under accession code 3ITN.

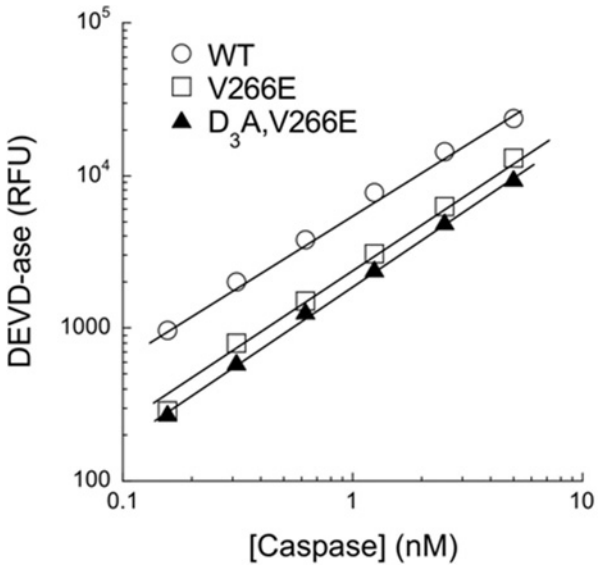

Figure S1 Dilution studies of the V266E interface mutants

The indicated caspase-3 proteins were diluted in standard assay buffer at concentrations between 0.15 and 10 nM and incubated for 15 min at 37 °C. The enzymatic activity was determined against 100 μM Ac-DEVD-AFC.

group was removed using 20 % piperidine in DMF and, after washing with DMF, dichloromethane, THF (tetrahydrofolate) and methanol, the resin was dried in vacuum. The resin was distributed in 75 mg portions into 57 wells of a 96-deep-well plate (semi-automatic FlexChem synthesizer). Standard peptide synthesis was used to prepare the libraries. The amino acid or mixture of amino acids, HOBt and DICI were preincubated for 4 min and added to the appropriate wells and agitated for 3 h along with 30 min Fmoc decouplings in 20 % piperidine in DMF. The variable amino acid mixtures were prepared as an isokinetic mixture with 19 amino acids (all amino acids omitting cysteine and methionine due to the oxidation problems; norleucine was used to mimic methionine). The N-termini of the tetrapeptides were capped with acetate (Ac_2O and DIEA in DMF) for 2 h. The resin was washed with DMF, dichloromethane, THF and methanol, and the resin was dried in vacuum for 24 h. The cleavage of the substrates was carried out for 1.5 h at room temperature using the mixture of 92.5 % TFA (trifluoroacetic acid), 2.5 % water, 2.5 % tri-isopropyl silane and 2.5 % phenol (1.5 ml per well). After cleavage, TFA was removed and the substrates were precipitated for 10 min at 0 °C using t-butyl-methyl ether (12 ml) and centrifuged. This step was repeated once. Subsequently, all ACC substrates were dissolved in water/dioxane (1:1, v/v) and freeze-dried for 48 h. Finally, all individual substrates were dissolved as stock solutions at concentration of 50 mM in biological purity DMSO and stored frozen.

RT–PCR

HEK-293A cells, transfected with caspase-3 mutants and in the presence of 100 μM ZVAD-FMK, were harvested and lysed in TRizol® reagent (Invitrogen). The total RNA was extracted using TRizol® as recommended by the manufacturer's instructions and resuspended in 50 μl of DEPC-treated water. Contaminating genomic/plasmidial DNA was removed from the total RNA solution by using the DNase free kit (Ambion). To prepare the first strand cDNA, ~1 μg of (DNA-free) RNA was primed with oligo(dT) and subjected to RT in 20 μl final volume by using the SuperScriptIII kit from Invitrogen. Control reactions did not include the reverse transcriptase enzyme in the reaction mixture. All cDNA samples (~200 ng) were amplified by PCR using either caspase-3-specific primers (forward: caspase-3 internal primer; reverse: FLAG-tag primer) or primers designed to amplify a housekeeping gene such as α-tubulin. Samples were run in 0.8 % agarose gel and stained with ethidium bromide. The DNA molecular ladder was from Invitrogen (DNA 1 kb plus).

Cell lysate preparation

HEK-293A or MCF7 cells were harvested as described above, washed with PBS, and the cell pellet was frozen at −20°C for a maximum of 3 days. Thawed cell pellets were lysed on ice for 10 min with mRIPA buffer [modified radioimmunoprecipitation buffer; 10 mM Tris/HCl, pH 7.4, 150 mM NaCl, 1 % (v/v) Nonidet P40, 0.5 % deoxycholate,

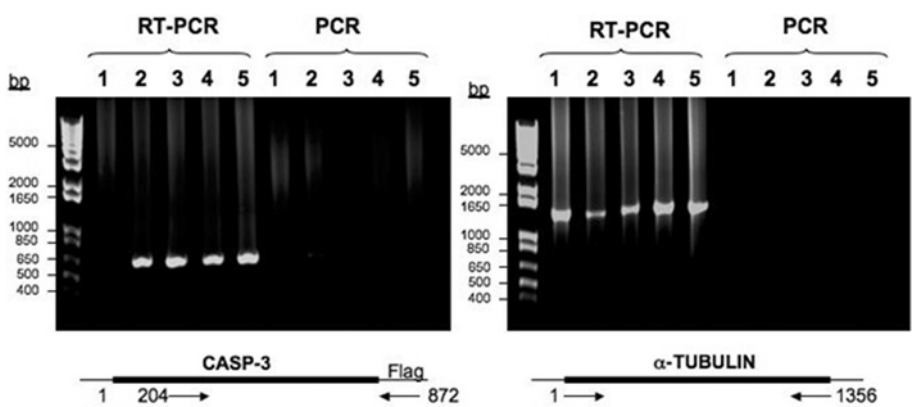

Figure S2 RT–PCR reactions of DNA-free RNA isolated from transfected HEK-293A cells

The following FLAG-tagged constructs were used: 1, vector control; 2, caspase-3 (WT); 3, procaspase-3(D_3A); 4, caspase-3(V266E); 5, procaspase-3(D_3A,V266E). The PCR reactions used specific primers for caspase-3–FLAG and α-tubulin, depicted at the bottom of each panel. To rule out the possibility of plasmidial/genomic DNA contamination, control reactions (PCR) used RNA samples subjected to RT reactions in the absence of the reverse transcriptase.

0.1 % SDS and 5 mM EDTA] containing the following protease inhibitors: 50 μM DCI (dichloroisocoumain), 50 μM leupeptin, 50 μM MG132 and 10 μM E-64. Lysates were clarified by centrifugation at 15 000 ***g*** for 15 min. For preparation of hypotonic Jurkat lysates, cells were treated as described previously [6]. Jurkat lysates were immunodepleted for caspase-3 by incubation with caspase-3 antibodies diluted 1:100 (BD clone 19) overnight at 4 °C, followed by the addition of Protein A/G beads for 2 h [7]. Depleted Jurkat cell lysates were reconstituted with recombinant caspase-3 mutants (25 nM final concentration) and incubated at 37 °C to allow caspase substrate processing. The lysates were balanced for protein content before immunoblotting.

Caspase assays

The protein concentrations in the cell lysates were determined using the Bio-Rad DC protein assay, and the lysates were normalized for protein content. To determine the activity of the executioner caspases, cell lysates were diluted 1:5 in caspase assay buffer [10 mM Pipes, pH 7.4, 150 mM NaCl, 0.1 % CHAPS, 10 % (w/v) sucrose and 10 mM DTT], incubated for 15 min at 37°C, and then the rate of hydrolysis of fluorogenic substrate (Ac-DEVD-AFC, 100 μM) was measured. For inhibition studies using XIAP, the recombinant caspase-3 proteins (300–600 pM) were incubated for 30 min at 37 °C in modified caspase buffer [50 mM Hepes, pH 7.4, 100 mM NaCl, 10 % (w/v) sucrose, 0.1 % CHAPS, 20 mM 2-mercaptoethanol] with serial dilutions of XIAP (0–700 nM). Residual activity was determined by the rate of hydrolysis of Ac-DEVD-AFC (100 μM) with an f_{MAX} Fluorescence Plate Reader (Molecular Devices). The apparent inhibition constant $K_{i,app}$ or the IC_{50} was determined from the uninhibited rate (v_o) and inhibited rates (v_i), by plotting the percentage of inhibition ($100 \times v_i/v_0$) against inhibitor concentration [I] as shown in eqn 1:

$$100 \times \frac{v_i}{v_0} = b + \frac{(100 - b) \times K_{i,app}}{K_{i,app} + [I]} \quad (1)$$

where b is the baseline of inhibition at infinite inhibitor concentration. The value for baseline b approaches zero for strict competitive inhibition and is more than 5–10 for mixed

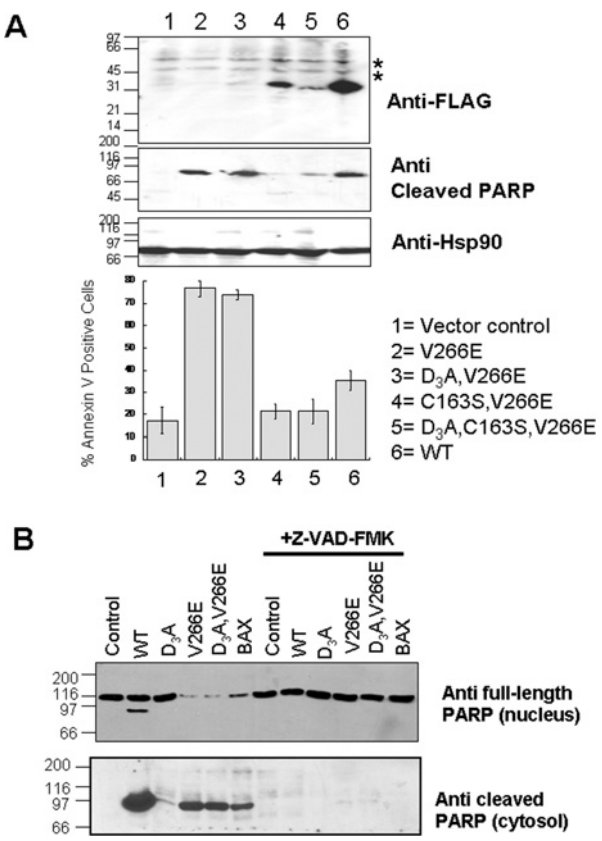

Figure S3 Inactive V266E variants no longer support apoptosis

(**A**) Western blots (upper panels) of cellular lysates from cells transfected with inactive variants of V266E mutants (lower panel). Protein expression and activation was assessed by antibodies against the FLAG tag, for detection of the transfected constructs, or cleaved PARP. Hsp90 panel represents a loading control; *non-specific protein. (**B**) Western blots of the cellular lysates from Figure 2(A) against anti-full-length PARP (nuclear extract) or cleaved PARP (cytosolic extract).

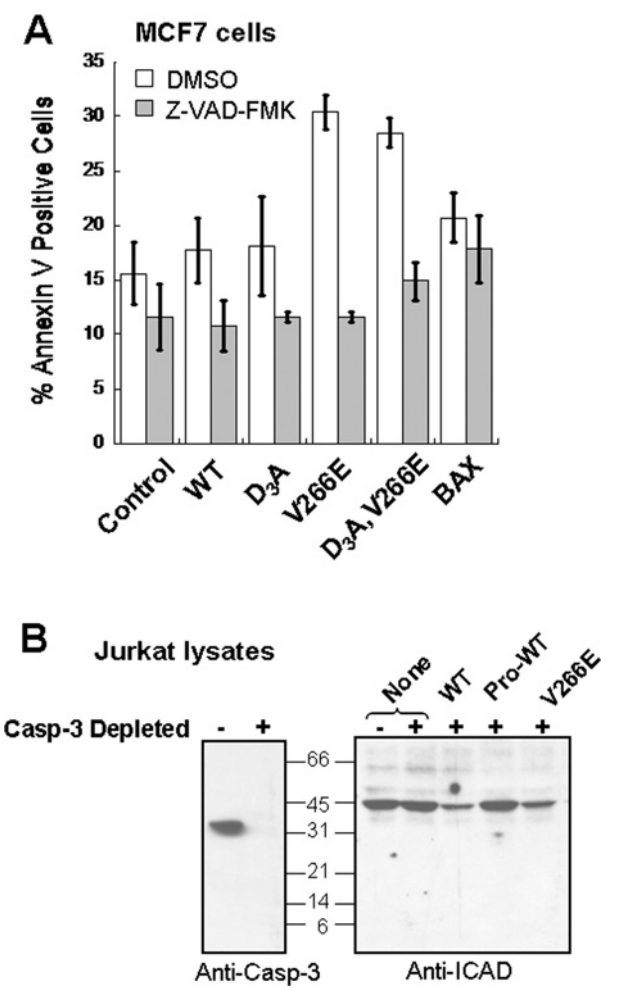

Figure S4 Caspase-3 V266E mutants kill cells independently of the presence of endogenous caspase-3

(**A**) MCF7 cells, which lack procaspase-3, were transfected with 1 μg of total DNA, as described in the legend for Figure 2 of the main text, and 24 h later the cells were quantified by FACS for Annexin V-positive cells. The values represent the means $\pm$ S.D. for three independent experiments. (**B**) Hypotonic Jurkat lysates were immuno-depleted of endogenous caspase-3 (Casp-3 Depleted) and reconstituted with recombinant caspase-3. After incubation at 37 °C, cleavage of ICAD was detected by immunobloting for full-length ICAD.

inhibition. From the Michaelis–Menten constant, K_M, of each caspase mutant for the substrate Ac-DEVD-AFC and substrate concentration [S], the true K_i of inhibition was calculated using eqn 2:

$$K_i = \frac{K_{i,app}}{1 + \frac{S}{K_M}} \quad (2)$$

For inhibition studies using p35, the experiments were carried out as above, except that the concentration of caspase-3 was 2 nM and that of p35 varied between 0 and 12 nM.

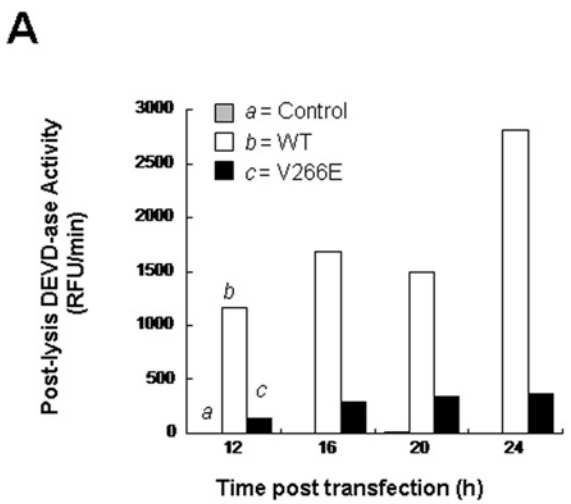

Figure S5 Relative DEVD-ase activity

(**A**) DEVD-ase activity in lysates prepared from cells transfected with WT or V266E for the indicated time periods. (**B**) DEVD-ase activity in culture medium from cells transfected with caspase-3 mutants. Cultures grown in complete growth medium were centrifuged at 500 ***g*** to remove the cells. Supernatant (25 μl) was mixed with 2× assay buffer (25 μl), incubated at 37 °C for 10 min, and the DEVD-ase activity was measured as described in the Experimental section. The activity was normalized to the volume of the cell culture (~ 2.5 ml), but not to the amount of protein from the cell lysates (see Figure 3 of the main text). The y-axis values for DEVD-ase activities generated by cell medium and the cell lysates (see Figure 3 of the main text) are not comparable. RFU, relative fluorescence units.

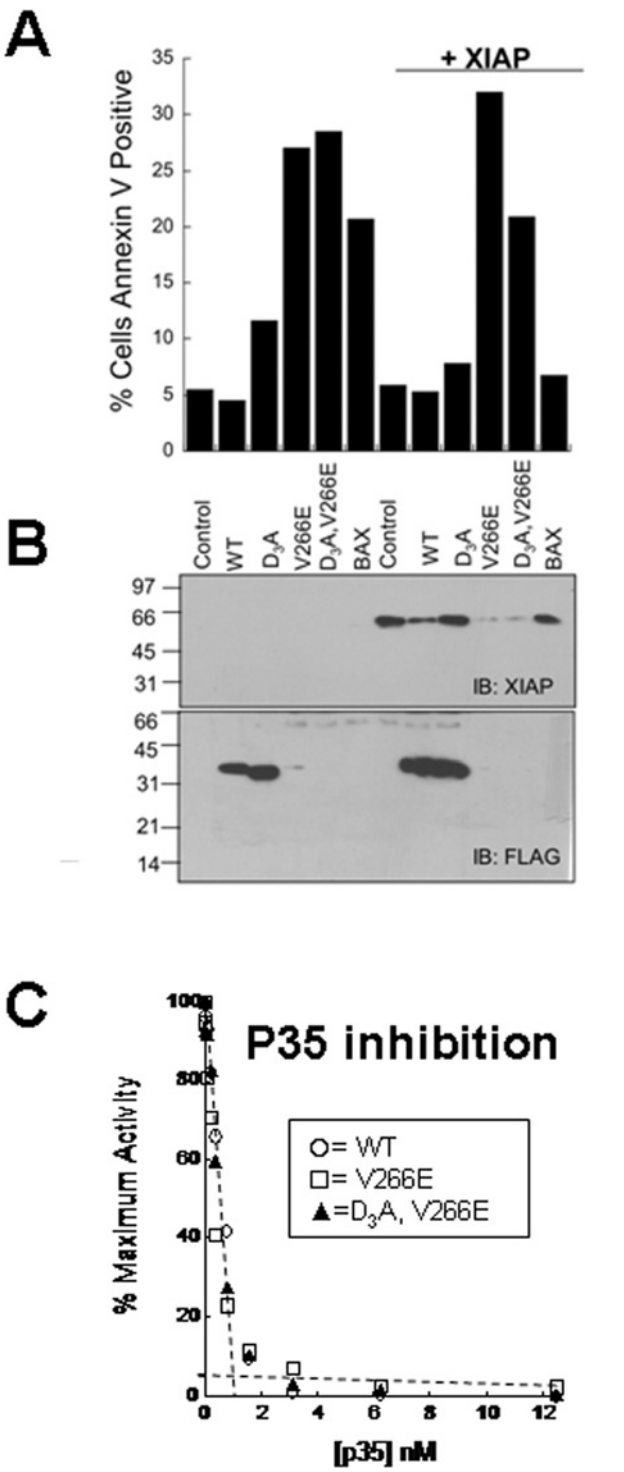

Figure S6 Co-expression of XIAP with the caspase-3 V266E mutants cannot rescue cells from apoptosis

(**A**) HEK-293A cells were transfected with 2 μg of total DNA (1 μg of caspase DNA plus 1 μg XIAP DNA for co-transfections) and, after 24 h, the cells were quantified for Annexin V staining. We note that the values for V266E and D_3A,V266E in the presence of XIAP are not significantly different given the error limits for this experiment. (**B**) Western blot analysis of the samples from (**A**) shows that XIAP does not accumulate in cells containing the caspase-3 V266E mutants. (**C**) All caspase-3 mutants (2 nM) were efficiently titrated with the viral inhibitor p35 at concentrations as low as those approaching the $K_{i,app}$ for inhibition.

Procaspase-3 homology models, energy minimization and molecular dynamics

Models of both the inactive and active procaspase-3 proteins were built as described below, and the program CHARMm version 27 [8] was used for molecular dynamics simulations and energy minimizations to assure that the final models represent energetically feasible structures.

The inactive procaspase-3 model was generated using the alignment mode of the SWISS-MODEL protein structure homology modelling server [9]. The target sequence, procaspase-3, was modelled using procaspase-7 (PDB code 1K88) as the template sequence. ϕ and ψ angles were corrected manually with COOT [10] so that all dihedral angles throughout the entire structure were within accepted values in the Ramachandran plot (see Table S1). The IL in molecule B of procaspase-7 is mostly, but not completely, ordered, such that residues 167–177 (procaspase-3 numbering) are not visible in the electron density maps. It was therefore necessary to build the missing residues in order to obtain the structure of the complete IL. Given the degrees of freedom available for the missing residues in the linker, we acknowledge that our initial model included one of several possible conformations for the missing section. The starting conformation is one in which each additional residue was built to have Φ and ψ angles in optimal regions in the Ramachandran plot, as monitored by the appropriate function in the program COOT, although at the same time connecting the two ends of the IL already present in the model.

The model of active procaspase-3(V266E) was built with the wild-type caspase-3 structure as the template (PDB code 2J30). This is appropriate due to the high levels of activity of D_3A,V266E. On the basis of our previous results [11], Asp^{169} and Val^{189} were used as anchor points, and the IL was built manually using COOT. ϕ and ψ angles were inspected manually during the initial building of the IL, as was performed for the model of the inactive protein. In this case, however, the side chains for the built residues have substantial degrees of freedom and were given common rotamers. The backbone was built over the interface in order to connect the two ends of the IL in a way to form the loop bundle of both active sites, as is observed in active caspase-3.

After the initial building of the two models, any strains or unfavourable conformations were relieved using the CHARMm potential energy function with the PARAM19 parameter set for extended atom representation and an atom-based force switching function applied to non-bonded interactions, with the switch starting at 5 Å and ending at 6 Å. All energy minimizations were performed using a gradient tolerance cutoff of 0.0001.

The initial models were placed in equilibrated 62 Å cubes of TIP3P [12] water molecules, and all atoms within 2.6 Å of any protein atom or crystallographic water molecule were deleted on a group-wise basis. This resulted in a protein solvated by 5417 and 5325 water molecules for the inactive and active models respectively. All calculations were performed with periodic boundary conditions. Bonds containing hydrogen were constrained to their equilibrium bond lengths using the SHAKE algorithm [13]. Energy minimization was achieved using a combined approach of 100 steps of steepest descent followed by 1000 steps of conjugate gradient. Each model was then subject to 10 ps of molecular dynamics simulations at 1000 K with a representative structure saved every 1 ps during the trajectory. The elevated temperature was for greater sampling of conformational space. The leapfrog Verlet algorithm was used for numerical integration of Newton's equations of motion at 0.001 ps intervals. The ten structures saved during each trajectory were energy minimized with 100 steps of steepest descent. The ILs in the resulting ten models of the inactive procaspase-3 and active procaspase-3 showed a main chain RMSD (root mean square deviation) of 0.308 Å and 0.244 Å respectively, demonstrating that at least within the radius of convergence given by our simulation conditions there is a single overall conformation of the IL in each case.

Comparison of the final model of inactive procaspase-3 with the procaspase-7 template using the brute force alignment in LSQMAN [14] resulted in an overall RMSD of 0.416 Å, demonstrating good agreement between the target structure and the model. Similarly, the RMSD between our model of the active procaspase-3(V266E) and the wild-type caspase-3 template is 0.226 Å, excluding the L2′ residues, which must differ in the two structures due to its connectivity to the rest of the IL in procaspase-3 and its positioning in the active site in the adjacent heterodimer in the mature caspase-3 dimer.

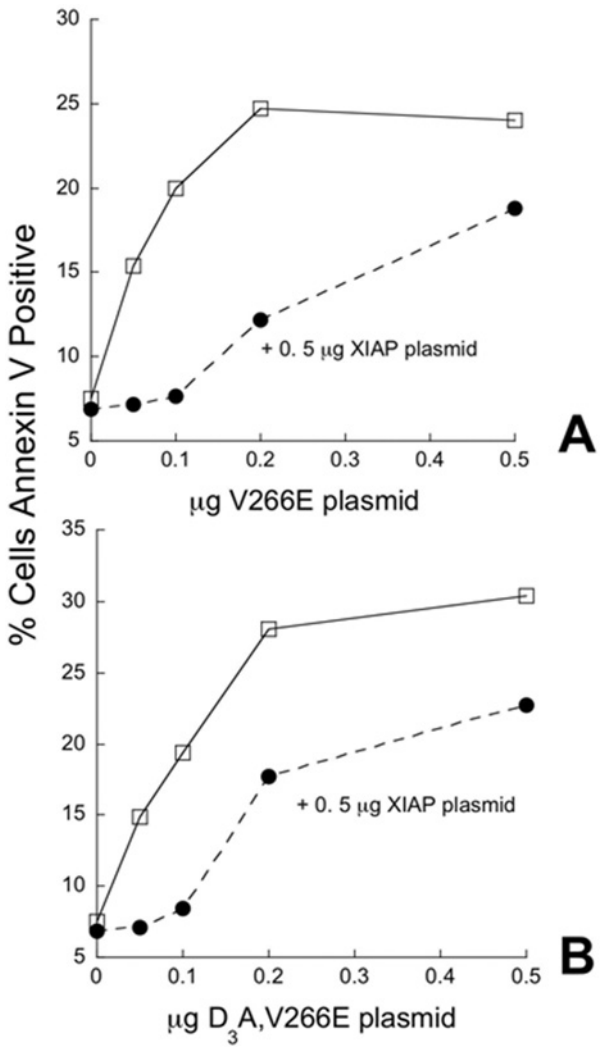

Figure S7 Poor inhibition of caspase-3 interface mutants by XIAP

(**A**) Co-transfection of caspase-3(V266E) with XIAP at various DNA ratios. (**B**) Co-transfection of caspase-3(D_3A,V266E) with XIAP at various DNA ratios. Transfections were performed with increasing amounts of caspase-3 vector in the presence of a constant amount of XIAP vector (●). The control in the absence of XIAP is shown as □. Cells were quantified by FACS for Annexin V staining 20 h post-transfection.

Table S1 Summary of data collection and refinement statistics for caspase-3(V266E)

Space group	I222			
Unit cell	a = 69.224 Å b = 84.607 Å c = 96.171 Å $\alpha = 90°$ $\beta = 90°$ $\gamma = 90°$			
Temperature (K)	100			
Resolution (Å)	1.63			
Number of reflections	41720			
Completeness (%)	99			
Redundancy	3.0			
R_{sym} (%)[a]	11.1			
Average I/σ	17.8 (6.1)			
R_{work} (%)[b]	20.17			
R_{free} (%)[c]	23.54			
RMSD for bond lengths (Å)	0.005			
RMSD for bond angles (Å)	1.2			
Number of protein atoms	1939			
Number of water molecules	297			
Ramachandran statistics				
	WT	V266E	Procaspase-3 (inactive)	Procaspase-3 (active)
In preferred regions	235 (96.7%)	233 (97.9%)	416 (88.1%)	452 (93.4%)
In allowed regions	5 (2.1%)	5 (2.1%)	47 (10%)	28 (5.8%)
Outliers	3 (1.2%)	0 (0%)	9 (1.9%)	4 (0.8%)

[a] $R_{sym} = \sum |Ii - < I > | / \sum I$

[b] $R_{work} = \sum ||F_0| - |F_c|| / \sum |F_0|$, calculated by using 90 % of the reflections against which the model was refined.

[c] $R = \sum ||F_0 - |F_c|| / \sum |F_0|$, calculated by using a test set consisting of 10 % of the total reflections, randomly selected from the original data set.

REFERENCES

1 Pop, C., Feeney, B., Tripathy, A. and Clark, A. C. (2003) Mutations in the procaspase-3 dimer interface affect the activity of the zymogen. Biochemistry **42**, 12311–12320

2 Stennicke, H. R., Jurgensmeier, J. M., Shin, H., Deveraux, Q., Wolf, B. B., Yang, X., Zhou, Q., Ellerby, M., Ellerby, L. M., Bredesen, D. et al. (1998) Pro-caspase-3 is a major physiologic target of caspase-8. J. Biol. Chem. **273**, 27084–27090

3 Janicke, R. U., Sprengart, M. L., Wati, M. R. and Porter, A. G. (1998) Caspase-3 is required for DNA fragmentation and morphological changes associated with apoptosis. J. Biol. Chem. **273**, 9357–9360

4 MacKenzie, S. H. and Clark, A. C. (2008) Targeting cell death in tumors by activating caspases. Curr. Cancer Drug Targets **8**, 98–109

4a Dechene, M., Wink, G., Smith, M., Swartz, P. and Mattos, C. (2009) Multiple solvent crystal structures of ribonuclease A: an assessment of the method. Proteins **76**, 861–881

5 Maly, D. J., Leonetti, F., Backes, B. J., Dauber, D. S., Harris, J. L., Craik, C. S. and Ellman, J. A. (2002) Expedient sold-phase synthesis of fluorogenic protease substrates using the 7-amino-4-carbamoylmethylcoumarin (ACC) fluorophore. J. Organic Chem. **67**, 910–915

6 Cullen, S. P., Luthi, A. U. and Martin, S. J. (2008) Analysis of apoptosis in cell-free systems. Methods **44**, 273–279

7 McStay, G. P., Salvesen, G. S. and Green, D. R. (2008) Overlapping cleavage motif selectivity of caspases: implications for analysis of apoptotic pathways. Cell Death Differ. **15**, 322–331

8 Brooks, B. R., Bruccoleri, R. E., Olafson, B. D., States, D. J., Swaminathan, S. and Karplus, M. (1983) CHARMM: A program for macromolecular energy, minimization, and dynamics calculations. J. Comp. Chem. **4**, 187–217

9 Arnold, K., Bordoli, L., Kopp, J. and Schwede, T. (2006) The SWISS-MODEL workspace: a web-based environment for protein structure homology modelling. Bioinformatics **22**, 195–201

10 Emsley, P. and Cowtan, K. (2004) COOT: model-building tools for molecular graphics. Acta Crystallogr. Sect. D Biol. Crystallogr. **60**, 2126–2132

11 Feeney, B., Pop, C., Swartz, P., Mattos, C. and Clark, A. C. (2006) Role of loop bundle hydrogen bonds in the maturation and activity of (pro)caspase-3. Biochemistry **45**, 13249–13263

12 Jorgensen, W. L., Chandrasekhar, J., Madura, J. D., Impey, R. W. and Klein, M. L. (1983) Comparison of simple potential functions for simulating liquid water. J. Chem. Phys. **79**, 926–935

13 Ryckaert, J. P., Ciccotti, G. and Berendsen, H. J. C. (1977) Numerical integration of the cartesian equations of motion of a system with constraints: molecular dynamics of n-alkanes. J. Comp. Phys. **23**, 327–341

14 Kleywegt, G. J. (1996) Use of non-crystallographic symmetry in protein structure refinement. Acta Crystallogr. Sect. D Biol. Crystallogr. **52**, 842–857

Received 29 May 2009/8 September 2009; accepted 30 September 2009
Published as BJ Immediate Publication 30 September 2009, doi:10.1042/BJ20090825